(4)

AFGL-TR-88-0100

Scattering Under Pasadena, California

Charles A. Langston
Roy J. Greenfield

Pennsylvania State University
114 Kern Building
University Park, PA 16802

1 April 1988

Scientific Report No. 1

APPROVED FOR PUBLIC RELEASE; DISTRIBUTION UNLIMITED

AIR FORCE GEOPHYSICS LABORATORY
AIR FORCE SYSTEMS COMMAND
UNITED STATES AIR FORCE
HANSCOM AIR FORCE BASE, MASSACHUSETTS 01731-5000

Unclassified

SECURITY CLASSIFICATION OF THIS PAGE

REPORT DOCUMENTATION PAGE

1a. REPORT SECURITY CLASSIFICATION: Unclassified	1b. RESTRICTIVE MARKINGS
2a. SECURITY CLASSIFICATION AUTHORITY	3. DISTRIBUTION/AVAILABILITY OF REPORT: Approved for public release; distribution unlimited
2b. DECLASSIFICATION/DOWNGRADING SCHEDULE	
4. PERFORMING ORGANIZATION REPORT NUMBER(S)	5. MONITORING ORGANIZATION REPORT NUMBER(S): AFGL-TR-88-0100
6a. NAME OF PERFORMING ORGANIZATION: Pennsylvania State University; 6b. OFFICE SYMBOL (If applicable)	7a. NAME OF MONITORING ORGANIZATION: Air Force Geophysics Laboratory
6c. ADDRESS (City, State and ZIP Code): 114 Kern Building, University Park, PA 16802	7b. ADDRESS (City, State and ZIP Code): Hanscom AFB, Massachusetts 01731
8a. NAME OF FUNDING/SPONSORING ORGANIZATION: AFGL; 8b. OFFICE SYMBOL (If applicable)	9. PROCUREMENT INSTRUMENT IDENTIFICATION NUMBER: F19628-87-K-0024
8c. ADDRESS (City, State and ZIP Code): Hanscom AFB, MA 01731	10. SOURCE OF FUNDING NOS: PROGRAM ELEMENT NO. 61101E; PROJECT NO. 7A10; TASK NO. DA; WORK UNIT NO. CN
11. TITLE (Include Security Classification): Scattering Under Pasadena, California	
12. PERSONAL AUTHOR(S): Langston, Charles A.; Greenfield, Roy J.	
13a. TYPE OF REPORT: Scientific No. 1; 13b. TIME COVERED: FROM 2/01/87 TO 1/31/88; 14. DATE OF REPORT (Yr., Mo., Day): 1988 April 1; 15. PAGE COUNT: 96	
16. SUPPLEMENTARY NOTATION	
17. COSATI CODES: FIELD / GROUP / SUB GR	18. SUBJECT TERMS (Continue on reverse if necessary and identify by block number): Scattering, Teleseismic Body Waves, CODA Q, Anelasticity, Receiver Functions, Ps Conversions

19. ABSTRACT (Continue on reverse if necessary and identify by block number)

Teleseismic receiver functions for structure under PAS (Pasadena, CA) are derived from azimuthally-distributed teleseismic P waves recorded on Benioff 1-90 instrumentation. The broad-band three-component Benioff 1-90 system is peaked at one sec period and allows resolution of major crustal interfaces from large Ps conversions seen in the receiver function data. The observed body wave data are quite complex showing exceptionally large Ps conversions and scattered waves on horizontal components. Radial and tangential motions are of equal magnitude and show major off-azimuth converted Ps waves suggesting large scale crustal heterogeneity beneath the station. Stochastic simulations of 1D plane layered structure show that geologically unreasonable 1D models are required to fit the data. The observed coda decay yields a scattering Q estimate of 230 at 2 sec period using an energy flux model for a propagating plane wave interacting with a scattering layer over a homogeneous halfspace. Observed and synthetic coda decay follows the theoretical exponential decay predicted by the model and is due entirely to

20. DISTRIBUTION/AVAILABILITY OF ABSTRACT: UNCLASSIFIED/UNLIMITED ☐ SAME AS RPT ☒ DTIC USERS ☐	21. ABSTRACT SECURITY CLASSIFICATION: Unclassified
22a. NAME OF RESPONSIBLE INDIVIDUAL: James Lewkowicz	22b. TELEPHONE NUMBER (Include Area Code): (617) 377-3028; 22c. OFFICE SYMBOL: AFGL/LWH

DD FORM 1473, 83 APR EDITION OF 1 JAN 73 IS OBSOLETE

Unclassified

SECURITY CLASSIFICATION OF THIS PAGE

19. ABSTRACT

diffusion of coda energy out of the layer into the halfspace. PAS coda is compared to coda from deep teleseisms recorded at SCP (State College, PA) and it is seen that scattering is more severe at PAS as reflected in higher coda levels and slower decay rate. Analysis of a major Ps conversion arriving 3 seconds after direct P indicates that a major crustal discontinuity at about 20 km depth dips at high angles to the north under the San Gabriel Mountains. This interface probably represents the crustal tectonic boundary between the Transverse ranges and the Los Angeles basin.

Table of Contents

List of Scientists Contributing to Report

C.A. Langston

List of Publications Resulting from Total or Partial Sponsorship

Vogfjord, K.S., and C.A. Langston (1987). The Meckering earthquake of 14 October 1968: A possible downward propagating rupture, Bull. Seism. Soc. Am., 77, 1558-1578.

Langston, C.A.(1987). Depth of faulting during the 1968 Meckering, Australia, earthquake sequence determined from waveform analysis of local seismograms, Jour. Geophys. Res., 92, 11,561-11,574.

Varadan, V.K., A. Lakhtakia, V.V. Varadan, and C.A. Langston(1987). Radiation characteristics of elastodynamic line sources buried in layered media with periodic interfaces.I. SH-wave analysis, Bull. Seism. Soc. Am., 77, 2181-2191.

Varadan, V.K., A. Lakhtakia, V.V. Varadan, and C.A. Langston(1987). Radiation characteristics of elastodynamic line sources buried in layered media with periodic interfaces.II. P- and SV-wave analysis, Bull. Seism. Soc. Am., 77, 2192-2211.

Report Summary

Task Objectives

The general objective of this research is to understand the factors important in shaping the seismic signature of small events recorded at local and regional distances. Specific objectives are 1) the identification of deterministic aspects of the wavefield from small earthquakes and explosions to allow the inference of source depth and other source parameters, and 2) to understand the effects of scattering and lithospheric heterogeneity on the propagation of high frequency regional phases. The combined analysis of "deterministic" and "stochastic" wave propagation effects is required to unravel the complexity of regional phases for the purposes of event discrimination.

Technical Problem

Regional phases from small events are affected by complex interactions between source radiation and wave propagation effects due to structure in the crust and upper mantle. Because observations are confined to the high frequency band (>2 hz), lithospheric heterogeneity becomes important in shaping high frequency regional phases. Typical wave lengths are much shorter than the total travel path and are comparable to known geologic structure.

An aspect of the problem of regional wave propagation is examined here involving the nature of coda associated with major arrivals. Simple wholespace scattering models are often applied to the coda of regional S phases to deduce scattering or anelastic attenuation. The level and amplitude decay of coda is a characteristic of the data which seems to be robust for particular regions and can be used to deduce source magnitude, once calibrated. Factors affecting the level of scattering near the source and near the receiver are also obviously important in yield estimation problems and waveform modeling for source parameters. It is important, therefore, to investigate the major assumptions contained in these wholespace models and to determine which are appropriate. This was done by simplifying the wave propagation regime of a source in a scattering medium to that of the plane wave incident to heterogeneous structure under a receiver. Observed coda in broad-band teleseismic receiver functions was simulated through computation of synthetic seismograms for 1D stochastic structures and through the construction of energy flux models for wave propagation in a scattering layer over a homogeneous halfspace. The results suggest that the gross geometry of the scatterers is very important to the problem of coda decay and coda level and that wholespace models significantly misrepresent the coda.

General Methodology

Broad band data from deep earthquakes recorded at the stations PAS (Pasadena, CA) and SCP (State College, PA) were analyzed from a point view that the coda behind direct P was due to

wave scattering in a heterogeneous medium under the respective receivers. The data at PAS written by simple, deep earthquakes show very complex, high amplitude, and long duration coda. An analysis of Ps conversions in the first 10 seconds of the waveforms shows that structure under the station is three-dimensional since significant particle motions occur out of the sagittal plane of the ray. Of interest to this discussion is the nature of scattering induced by complex structure and the formation of P coda.

Plane layered stochastic structure models were constructed using a random number generator with an exponential spatial correlation function and a correlation length of 1 km (e.g., Frankel and Clayton, 1986). This was done to explore the degree of 1D heterogeneity required to mimic the observed data. Synthetic seismograms for an incident P plane wave under the randomly layered models were constructed using the Thompson-Haskell technique.

An energy flux model was developed for the plane wave response of a scattering layer over a homogeneous halfspace. This was done to explain aspects of the 1D simulations as well as parameterizing the receiver function data. The major assumptions in the model are based on conservation of energy, homogeneity of the coda field within the layer and leakage of coda energy into the halfspace following a simple diffusion law. Justification for these assumptions are based on published numerical experiments (Frankel and Wennerberg, 1987) and observations of coda behavior in small regional earthquakes (Aki and Chouet, 1975; Dainty and Toksoz, 1977).

Technical Results

Summarizing the derivation, the coda amplitude is given by

$$A_C = \frac{\sqrt{I_D}}{\sqrt{t_d}} \; e^{+\omega t_d/2Q_s} \left(1 - e^{-\omega 2 t_d/Q_s}\right)^{\frac{1}{2}} e^{-\gamma t/2} \qquad (1)$$

where,

I_D = integral of the squared velocity of direct P

$t_d = h/\alpha$

h = layer thickness

α = P wave velocity

ω = circular frequency

Q_s = scattering Q

γ = diffusion constant for layer boundary.

Equation (1) shows that for the incident plane wave, the time dependence of the coda is controlled entirely by the diffusion constant of coda energy diffusing out of the layer into the halfspace. Wholespace energy flux models have coda decay controlled by the expansion of the volume behind the wavefront. Single scattering models have decay controlled by scattering Q. The theory predicts the form of coda decay seen in data and stochastic simulations quite accurately. Coda decay in wholespace models is only a result of scattering or anelastic attenuation.

Important Findings and Conclusions

Analysis of coda in teleseismic receiver functions suggests that there are other mechanisms which control the formation and decay of scattered coda waves which are separate from intrinsic or scattering attenuation. In particular, the simple geometry of an elastic scattering layer over halfspace produces coda decay which would be interpreted as an attenuation effect but is due to the simple redistribution of scattered energy from the layer to the halfspace. Such effects can be studied first by analyzing coda from teleseismic events at a receiver or array and then applying the parameters of the layer model to an appropriate energy flux model for a source contained within the layer.

Significant Hardware Development

N/A

Special Comments

N/A

Implications for Further Research

Scattering Q models are based on a number of assumptions concerning the distribution of the reservoir of energy contained in the scattered field. Further research will concentrate on combined application of teleseismic scattering determiniations and regional phase scattering. This combined analysis may offer constaints on scattering physics not obtainable by analysis of each data set alone. Results of this research will have important implications on studies of regional phase propagation, discrimination of small events, and yield estimation problems.

Scattering Under Pasadena, California

by

Charles A. Langston

1 April 1988

Department of Geosciences
Pennsylvania State University
University Park, PA 16802

Abstract

Teleseismic receiver functions for structure under PAS (Pasadena, CA) are derived from azimuthally-distributed teleseismic P waves recorded on Benioff 1-90 instrumentation. The broad-band three-component Benioff 1-90 system is peaked at one sec period and allows resolution of major crustal interfaces from large Ps conversions seen in the receiver function data. The observed body wave data are quite complex showing exceptionally large Ps conversions and scattered waves on horizontal components. Radial and tangential motions are of equal magnitude and show major off-azimuth converted Ps waves suggesting large scale crustal heterogeneity beneath the station. Stochastic simulations of 1D plane layered structure show that geologically unreasonable 1D models are required to fit the data. The observed coda decay yields a scattering Q estimate of 239 at 2 sec period using an energy flux model for a propagating plane wave interacting with a scattering layer over a homogeneous halfspace. Observed and synthetic coda decay follows the theoretical exponential decay predicted by the model and is due entirely to diffusion of coda energy out of the layer into the halfspace. PAS coda is compared to coda from deep teleseisms recorded at SCP (State College, PA) and it is seen that scattering is more severe at PAS as reflected in higher coda levels and slower decay rate. Analysis of a major Ps conversion arriving 3 seconds after direct P indicates that a major crustal discontinuity at about 20 km depth dips at high angles to the north under the San Gabriel Mountains. This interface probably represents the crustal tectonic boundary between the Transverse ranges and the Los Angeles basin.

Introduction

The analysis of teleseismic receiver functions represents an inexpensive and convenient way of imaging major crustal and upper mantle discontinuities under isolated receivers. The transmisivity of structure under a three-component seismometer is inferred from the timing and amplitude of Ps conversions seen on horizontal ground motions and is modeled to determine the location and velocity contrasts of the causitive interfaces (Burdick and Langston, 1977; Langston, 1979; Owens, 1984). The technique has been particularly useful in large scale structure studies using long-period body waves (e.g., Burdick and Langston, 1977; Langston and Isaacs, 1981; Hebert and Langston, 1985) to determine average crustal thickness and is increasingly being applied to broad-band, high-frequency data to obtain more resolution on structure (Owens, 1984; Owens et al, 1984; 1987).

One of the inevitable trade-offs in using higher frequency data is increased sensitivity to lateral heterogeneity in crustal structure. In one sense, this is desirable since a goal of such studies is to determine as much information about structure under the receiver as possible. However, it is also obvious that the wave field is severely spatially aliased through observations made at only a single surface point. Imaging procedures implicitely rely on modeling assumptions such as plane layering or, at most, simple curved interfaces. It is often observed that much of the wavefield is inaccessable to rational explanation using simple modeling techniques (Langston, 1979; Owens et al,1987). For example, receiver function data often display anomalous wave behavior such as P-wave particle motions which have significant tangential amplitudes.

A purpose of this paper is to examine strategies of treatment of broad-band receiver function data which take into account both stochastic and deterministic scattering effects due to heterogeneous structure. Structure under the station PAS (Pasadena, California) will be the focus of this effort. This station lies in

a geologically complex area of Southern California (Figure 1) and has had broad-band instrumentation over a long period of time. The study was initially motivated by simple observations of complex particle motions in the teleseismic P wave data (Lanester, 1977). The data were previously examined by Lee(1985) who attempted to model the receiver functions using dynamic ray tracing with models consisting of homogeneous layers separated by curved 3D interfaces. Lee's study was partially successful in explaining qualitative aspects of the data for early arrivals but he found that ray theory was inadequate to explain the high amplitude of inferred converted waves and the duration of signal.

In this paper, the receiver function data will be examined from two points of view. The first is from the standard method of treating the data to infer major velocity discontinuities under the station using "deterministic" aspects of the observed data and simple velocity models. Ps conversions from teleseismic P waves are found to be unusally large and are used to suggest the existence of a large velocity contrast interface in the lower crust which dips to the north under the San Gabriel Mountains.

The other point of view is to treat the data as resulting from an unknown scattering process and to attempt to infer the severity of wave scattering under the station. Using simple measures of the P coda amplitude decay along with 1D stochastic structure simulations, the question is asked: Are the data consistent with scattering due to reasonable plane layered structure? The negative answer for PAS suggests that such an analysis can be generally used to justify or not justify a research effort in modeling data with simple plane layered structure models. The severity of observed scattering under PAS also points out defeciencies in some simple scattering models and the need to develop appropriate models for 2 and 3D stochastic structures.

PAS Station and Regional Structure

PAS station has been in operation since the mid-1930's and has had a full complement of experimental long- and short-period instrumentation. Of interest to this study are the Benioff 1-90 (Seismometer Period = 1 sec, Galvonometer Period = 90 sec) and, to a lesser extent, the Press-Ewing 30-90 systems. The Benioff 1-90 system is peaked at 1 sec period but records across a wide frequency band comparable to the intermediate-period DWWSSN passband (see Appendix). Its nominal magnification of 3000 has allowed routine recording of teleseisms throughout its existence. Although the data are recorded in analog photographic format, the broad passband of the instrument potentially allows for significant time resolution of crustal Ps conversions. This potential, in conjunction with the recognized complexity of the receiver signal (Langston, 1977) as well as unusual tectonic problems associated with the Transverse Ranges Province of Southern California, motivates the present study of crustal structure under the receiver.

PAS station (Figure 1) lies near the southern boundary of the Transverse Ranges Province and the Los Angeles Basin - Peninsular Range Province. Geologic structure of the upper crust is known to be quite complex with major active faults separating regions of diverse rock type. For example, crystalline rocks of the San Gabriel Mountains a few kilometers north of PAS abut valley sediments that attain depths of up to 10 kilometers in the center of the Los Angeles Basin (Yerkes et al, 1965). The geology of the Transverse Ranges and the San Gabriel Mountains, in particular, suggests that much of the range is allochthonous being thrust over younger rocks of the Peninsular Range Province.

Hadley and Kanamori(1977) review a number of long-range refraction and travel time studies for the area and show that the Transverse Ranges are a locus of both upper mantle and crustal velocity anomalies. Using the Southern California Seismic Network, P delays from a PKIKP phase outlined an east-west

trending zone of higher than average velocities in the upper mantle. This zone was studied more extensively by Humphries et al(1984) using a tomographic imaging technique for teleseismic P waves recorded by the network. They determined that the vertical zone of high mantle velocities was contained within the Transverse range province and attained depths of at least 150 km. This zone was interpreted as a region of mantle down-welling analogous to a subduction zone but driven by relative movements of microplates making up the San Andreas fault system. In this model, upper crustal microplate movements are decoupled from lower crust and upper mantle structures with the result that the surface expression of the San Andreas fault is offset by a mid-crustal horizontal shear zone from the fault at depth.

The Transverse Ranges are also a locus of change in crustal structure between the western Peninsular Ranges - Los Angeles Basin and the Mojave Block to the east. Hadley and Kanamori (1977) suggest that a high-velocity lower crustal layer comprises about half of the crust in the Peninsular Ranges but tapers to only a few kilometers in the Mojave Block. Tomographic study of Pg and Pn waves in Southern California (Hearn and Clayton, 1986a;b) support this suggestion by showing slower average velocities in the Mojave Block relative to crust to the west. Crustal thickness from long-range refraction (Hadley and Kanamori, 1977) and time-term analysis (Hearn and Clayton, 1986b) suggest that the crust under PAS is about 31 km thick.

These studies demonstrate that structure in the area is quite complex. A major goal of the present work is to provide constraints on crustal thickness under this important transition between tectonic provinces as well as determining other structural details. Site-specific information provided by the receiver function technique will complement these broader crustal and upper mantle structure studies.

Data and Source Function Equalization

Waveform data from 21 teleseismic earthquakes were obtained from the seismogram archives of California Institute of Technology (Table 1). The seismograms were photographed and enlarged for hand digitization. Waveforms were digitized at an irregular sampling interval and interpolated to an equal sampling interval of 0.1 seconds. Processing included vector rotation of the horizontal components into the theoretical backazimuth of the P-wave arrival to obtain radial (positive away from the source) and tangential (positive clockwise around the source) ground motions.

A source function equalization procedure was then performed to remove the instrument response and unknown effective source function from the radial and tangential waveform data. In this procedure, the vertical component of motion is assumed to be free of any effect of near-receiver structure (reverberations, conversions) but contains the common instrument response and wave propagation effects from the mantle and near-source region. The data are time-windowed and Fourier transformed. The vertical spectrum is divided into the horizontal spectra and then multiplied by a Gaussian function to remove high frequency noise. The spectral division is also accompanied by prewhitening the vertical component spectra using a "water level" parameter to remove spurious spectral holes. The "water level" used for data considered here was 0.1% of the maximum of the vertical component amplitude spectrum. The Gaussian filter used is equivalent to a Gaussian pulse in the time domain with a half width of 1 second (i.e., a=1.67 in $e^{-a^2 t^2}$). Details and justification of use of the technique can be found in Langston(1979).

Figure 2 shows examples of waveform data for events in the three major backazimuth ranges, 128°, 235°, and 315°. Also shown are PKIKP waveforms of the 1/23/76 event which was also used in Hadley and Kanamori's (1977) study. This phase has unique properties in a receiver function study and will be used as a

powerful contraint on structure under the station. Note, that in all cases, the magnitude of tangential motions excited by the P wave is comparable to radial motions. In an ideal radially stratified earth, P and resulting P-SV conversions are restricted to the sagittal plane containing the ray. Note also that tangential and radial motions, or conversely, the observed horizontal components differ quite substantially in waveform suggesting that simple instrument miscalibration or magnification differences cannot give rise to these anomalous particle motions. The Appendix discusses the calibration of the Benioff 1-90 system and shows that plausible miscalibration is not a factor.

Waveforms for the PKIKP phase for the 01/23/76 event also show very anomalous particle motions. This phase is incident below the crust with an incident angle of about 4 degrees. Thus, it is about as close to a vertically propagating P plane wave as one can get in practice. Horizontal motions, however, are not near-zero. They are about half the size of the vertical P wave and both components are grossly different. Furthermore, this event has a backazimuth in which the observed EW component is almost perfectly radial, and the observed NS component, tangential. Observed differences cannot be the result of instrument miscalibration or numerical rotation error. The data of Figure 2 strongly suggest that heterogeneous three-dimensional structure is causing large scattering effects in the receiver function data.

Because of the location of major teleseismic source zones, the equalized radial and tangential component data were grouped into three backazimuth groups and stacked (see Table 1 for groupings). The stacking was done by shifting all traces to a common relative time based on the P first arrival and then averaging the waveforms. Waveforms for plus and minus one standard deviation about the mean at each sample point were also computed. The resulting waveform stacks are shown in Figure 3 with their standard deviations and a comparison of stacks from the three backazimuth groups are shown in Figure 4. A display of

this type yields information on the coherency of arrivals within the waveform and of the level of processing noise (Owens, 1984).

Only the first 15 seconds of the waveforms are shown in Figure 3. Obviously, the data of Figure 2 show major arrivals in the horizontal waveforms for at least 60 seconds. This poses a dilemma for structure models that can be considered. It is very difficult to get such arrivals from plausible plane layered models. This problem will be addressed in a later section. We will first concentrate on major initial arrivals.

Figure 3a shows the waveform stacks for events from a backazimuth of 128^{o}. The bounding envelope for $\pm$ one standard deviation is quite large for tangential motions and relatively large for arrivals after direct P on the radial component. A phase marked "Ps" on the radial stack is observed on the radial data from the other backazimuth groups. This Ps conversion is indistinct on the tangential data and is approaching noise level.

The other two backazimuth groups (Figure 3b and 3c) show remarkably large arrivals, however. The Ps conversion is roughly half the size of direct P on the radial components and is also resolvably large on the tangential components. Note also that the tangential components show that the direct P wave amplitude is variable within the noise of measurement. There is some hint that later arrivals in the waveforms are coherent but, as we will see, are problematical.

Figure 4 shows the stacks displayed together with P and Ps phases annotated. The working hypothesis is that this secondary phase is a direct P-to-SV conversion beneath the station. Its large size, relative to direct P, on all except the 128^{o} tangential stack is remarkable and can be directly seen in the data of Figure 2 (Also see Appendix). Figure 5 shows particle motion plots of the radial and tangential stacks for 315^{o} and 235^{o} backazimuths. Note that the direct P wave conforms to nearly radial motions as expected for ideal P particle motion, but that the Ps conversion has been rotated 45^{o} or more out of

the sagittal plane.

The magnitude of this effect is quite large. It is very difficult to produce such Ps arrivals from simple dipping interfaces that dip only a few degrees or have velocity contrasts typical of continental crustal models (Langston, 1977; Lee, 1983). The implication is that there is a major discontinuity under PAS which has high dip and or high S wave velocity contrast.

These arrivals are also directly evident in long-period data from the station. Figure 6 compares observed waveforms for the 11/29/74 event recorded on the Benioff 1-90 and Press-Ewing 30-90 systems at PAS. The data have been shifted to a common time base. The vertical components, although showing some scattered waves in the coda, are pulse-like and show one major P arrival. The NS 1-90 component is dominated by the Ps conversion. Direct P is a minor initial arrival. The 30-90 NS record shows that the Ps conversion (arrow) also dominates the long-period waveform. The EW components show the Ps conversion (arrows) but direct P, the first pulse, is larger. Nevertheless, the Ps conversion is evident having the effect of broadening the initial pulse by a factor of two compared to the vertical long-period P-wave and producing a "shoulder" on this pulse. This comparison of data recorded on two different seismometer systems demonstrates that the crustal structure responsible for these scattering effects is radical and that the effect is not an artifact of instrument miscalibration.

One last constaint on the occurrence of this major Ps conversion can be obtained from the data. Langston (1977, 1979) suggests that the amplitude and polarity behavior with azimuth of tangential Ps can constrain the direction and magnitude of interface dip. Unfortunately, the phase is only well developed in the 235^{o} and 315^{o} azimuth groups although it may be significant that it is poorly developed in the 128^{o} azimuth group. The PKIKP phase from the 1/23/76 event, however, offers some independent information in this regard.

Since this phase is nearly vertically propagating, any Ps conversion from a dipping interface will be contained in the plane of the ray and dip direction. This is self-evident from the geometry (Langston, 1977). Thus, a simple plot of particle motion of the Ps conversion will lead to a direct measurement of the dip direction. Figure 7 displays such a plot. The Ps conversion is the largest arrival on the NS component and is easily seen in the particle motion plot. Note that it is polarized almost perfectly northward. Because Ps is positive, relative to direct radial P on the waveform stacks of Figure 4, it is due to conversion from a higher to lower velocity as depth decreases. Taking the negative polarity of the PKIKP phase into account yields an absolute dip direction of northward for the postulated dipping interface. This is consistent with the tangential Ps polarities displayed by the 235^{o} and 315^{o} stacks.

Deterministic Modeling of the Ps conversion

Recent efforts in modeling receiver function data have concentrated in formal inversion of the data to obtain a plane layered crustal and upper mantle model (e.g., Owens et al, 1987). Characteristics of the Pasadena data set preclude this approach. Excessive duration and amplitude of the horizontal component coda and large tangential amplitudes all argue against finding reasonable plane layered models. This will be addressed below. Nevertheless, the distinct Ps conversion seen in the data must have important implications on the nature of structure under the station.

Figure 8 shows a comparison of observed and synthetic radial component waveforms. The radial stack for 235^{o} azimuth is shown below a synthetic radial seismogram computed for a crustal model proposed for the area by Hadley and Kanamori(1977). The Thompson-Haskell method (Haskell, 1962) was used to construct the synthetic. The crustal model is shown in Figure 9 with parameters tabulated in Table 2. The Moho occurs at 31 km depth and produces a moderately large Ps

conversion which arrives 4 seconds after direct P (shown by arrow in Figure 8). The observed Ps conversion is larger and arrives at least one second earlier. This is significantly earlier and suggests several possibilities.

First, if the Ps conversion is considered to be from the Moho, then the crust must be at most 27 km thick if Hadley and Kanamori's velocities are assumed. Hearn and Clayton's (1986a) imaging study using Pg waves suggested average crustal P wave velocities in the area of about 6.3 km/sec and a crustal thickness of about 31 km. It is possible that the receiver function data are sampling a local anomaly unresolved by Hearn and Clayton's data. Alternatively, if the crust is 31 km thick then average the average S wave velocity in the crust must be at least 4 km/sec. The average P wave velocity would also be correspondingly high at 6.9 km/sec assuming Poisson ratios near 0.25, appropriate for crustal rocks. These calculations were performed assuming plane wave propagation through a single layer crust over a mantle halfspace. In either case, in the event of a thin crust or a thicker high-velocity crust, there should be an anomalous mass excess in the crust and upper mantle column which would show up in the gravity field. No such anomaly is observed (Hadley and Kanamori, 1977).

One simple solution to the problem is to accept the average thickness and crustal velocities determined from previous studies and to infer a mid-crustal interface causing the large Ps conversion. A plane layered model which shows the general attributes of this working hypothesis is shown in Figure 9 (and Table 2) and the corresponding radial synthetic in Figure 8. Ps arrivals from the Moho are minimized by making the structure approximate a smooth gradient in that region. The large Ps relative amplitudes observed requires a high S-wave velocity contrast. This, in turn, implies a velocity inversion in the midcrust to attain the required large contrast. The synthetic shown in Figure 8 for this kind of low velocity zone (LVZ) structure shows the general characteristics of the data by approximating the arrival time and the double-peak character of the

arrival. The data may require that the LVZ be slightly shallower but the general characteristics are produced by the model.

Obviously, the plane layered model does not explain the anomalous particle motion of the Ps conversion. A series of ray theory calculations (Langston,1977) were performed to test the dipping interface model. The tangential Ps data require that the interface dip northward under the San Gabriel Mountains. Experience with such calculations indicates that there can be considerable trade-off between interface dip and velocity contrast (e.g., Langston, 1979). Waves which approach a dipping interface from the down-dip direction will have an effective angle of incidence which is larger than waves approaching a horizontal interface. This will produce a correspondly larger conversion. Of course, waves approaching from the up-dip direction will tend to have lower angles of incidence with less conversion.

A number of dipping interface models initially based on the Hadley and Kanamori crustal model of Table 2 were examined. The top of the 6.8 km/sec layer was allowed to dip up to 40^{o}. Two rays were traced through the model. These were direct P and the Ps conversion from the dipping interface. It was quickly seen that, although it may be possible to produce large Ps conversions for rays which approach the structure from the down-dip direction, models with dips greater than 10^{o} consistently produced low amplitude Ps conversions for rays traveling from the up-dip direction. Indeed, for P velocity contrasts of 6.2/6.8 and 5.0/6.8 (velocities in km/sec and assuming a Poisson solid), dips of 30^{o} resulted in Ps conversions which had opposite polarities relative to direct radial P. This is clearly inconsistent with the data which show large positive Ps conversions (Figure 4). Thus, interface dip is required to be of the order of 10^{o} or less. The S-wave velocity contrast is also required to be greater than 1 km/sec. The calculated Ps/P ratio for up-dip ray incidence is 0.19 for the 5.0/6.8 interface at 10^{o} dip. The observed Ps/P ratio for the 315^{o} stack is 0.57

(Figure 4) which represent waves coming up-dip but at an angle from the northward dip direction. Calculated tangential amplitudes for the Ps conversion are comparable to the radial amplitudes and agree with the 45° polarization anomaly seen in the data.

In summary Ps - P arrival times suggest that a major discontinuity occurs in the mid-crust under PAS. Although the polarity of radial and tangential Ps is consistent with the interface dipping northward under the San Gabriel Mountains, dip is of the order of 10^{0} or less and the S-wave velocity contrast must be unusually large (> 1 km/sec). Qualitatively, a major crustal low velocity zone can explain these observations but the extremely large Ps/P amplitude ratios probably imply that other factors are affecting the waveform such as ray focusing (Lee, 1983; Lee and Langston, 1983a;b).

Stochastic Structure Modeling

Up to this point, the data have been treated from a deterministic point of view. A discrete arrival was identified in the observed waveforms and modeled assuming it occurred at a well defined interface. The data show that the first Ps conversion is indeed a major wave propagation effect and it is reasonable to assume that major early arrivals will be due to direct interactions with discontinuities in the structure. However, if the data of Figure 2 are objectively examined it becomes clear that the inferred Ps conversion is simply the first of many large arrivals in the horizontal P-wave coda. Are these later arrivals fundamentally different from early arrivals? What do these large arrivals imply about the heterogeneity of the structure under the station?

The answer to these questions are probably beyond the scope of this study because of basic limitations in the data set and in knowledge of theoretical effects of wave propagation in heterogeneous structure. However, a slightly different question can be asked which can provide insight into the problem of the

large coda. Can plane layered structure mimic the coda seen in the data and, if so, what are the implications?

First we make the assumption that all arrivals seen after direct P in the data represent waves scattered in structure near the receiver. This assumption is probably poor for shallow earthquake sources simply because of known propagation effects like near-source surface reflections. Deep events, however, should be less affected by near-source scattering. A simple geometric argument can be made which requires that observed scattering occur near the receiver.

For deep teleseisms, tangential amplitudes in the coda are seen to be as large or larger than the vertical coda amplitude. Therefore, if these coda waves are due to scattering (P to P or S to P) in structure near the source they must finally convert to P waves to arrive soon after the direct P at the receiver. If they are P waves, they must have azimuth anomalies greater than 45^{0} since they are so large on the tangential component. This contradicts the near-source scattering hypothesis since the scattered waves themselves must come from teleseismic distances from the source. The conclusion is that it is possible that near-source scattering contributes to the effective teleseismic source function but that large horizontal coda amplitudes relative to horizontal P must be due to scattering near the receiver. This is basically the same argument used for the simple deterministic analysis of receiver functions. Cessaro and Butler(1987) have made similar comments in their analysis of tangential P seismograms.

Synthetic seismograms were computed for a series of receiver models with plane layered stochastic structure. The procedure used by Frankel and Clayton (1986) was adopted to generate a random velocity-depth function. This is summarized as follows:

1. A random series of normally distributed velocity values, v(z), with zero mean and unit variance was generated from a pseudo-random number generator. A

0.25 km sampling interval was assumed for a layer of thickness 30 or 60 km

2. The velocity function was Fourier transformed to the wavenumber domain to obtain v(k).

3. An exponential correlation function $N(z)=e^{-z/a}$ was assumed for the medium where a is the correlation length. The wavenumber spectrum of N(z), $\hat{N}(k)=2a/(1+k^2a^2)$, was used to filter v(z).

4. The filtered velocity spectrum was then inverse transformed and scaled to a wanted velocity variance and mean.

5. Synthetic seismograms were computed using the Thompson-Haskell method (Haskell, 1962).

Calculations were performed with a Gaussian correlation function as well, but the exponential correlation function proved to create somewhat more scattered arrivals since its spectrum is richer in higher wavenumbers. A correlation length, a, of one km was assumed. For 0.5 hz waves considered in this study, the corresponding value of k_za is approximately equal to 1, where k_z is the vertical component of the wavenumber. P-wave velocity-depth functions were computed using the random number generator and S wave velocities derived by assuming a Poisson solid. Density was held constant. Velocity parameters for the halfspace below the random crustal layer were generally set to those of the lowermost crustal layer.

The interest in this exercise is not to suggest that a particular correlation function is appropriate for earth structure under PAS but to investigate the degree of scattering required to mimic the observed data. The correlation function parameters were chosen to maximize 1D scattering effects within the chosen frequency band because the observed data show high amplitude coda. Frankel and Clayton(1986) suggest that a self-similar correlation function may be appropriate for earth structure since it gives a frequency independent Q over a broad frequency band and is consistent with array data. The receiver

function data set from PAS is essentially limited by the accuracy of hand digitization. We concentrate on examining coda formation near the peak of the instrument response which is accurately digitized

Two basic velocity models were considered in the 1D simulations. The first consisted of a heterogeneous crustal layer 30 km thick with a mean velocity of 5.5 km sec and velocity standard deviation of 10%. The top pair of waveforms in Figure 10 are typical examples of the free surface displacements computed from a number of realizations of the stochastic parameters. Figure 9 shows the corresponding velocity-depth functions for the lower and upper pair of synthetics. The incident wave time function assumed was the time derivative of the Gaussian function discussed above in the source equalization section. A quick glance at these synthetics and the data of Figure 2 show that synthetic coda levels are significantly lower than those observed and that the coda attenuates quickly with time.

It might be expected that a more realistic Moho with a large velocity contrast would trap more scattered energy in the crustal layer. The middle pair of synthetics shows this case for the model used to compute the upper synthetics but assuming a halfspace P wave velocity of 8 km/sec. Minor changes occur in the resulting synthetics. The largest change is to accentuate the Moho Ps conversion by about a factor of two (arrow). The coda is largely unaffected.

Increasing layer thickness tends to increase the duration of coda. Increasing the velocity standard deviation to 20% over a layer 60 km thick with a mean velocity of 6 km sec produces synthetic seismograms which start to mimic the data (bottom, Figure 10). Large Ps conversions and reverberations start to attain amplitudes comparable to the direct radial P-wave and coda duration superficially appears to agree with the observed data.

Thus, it appears that 1D velocity variations in excess of 20% over a significant thickness of the lithosphere are needed to mimic the receiver data at

PAS. Translated into a physical model, this suggests that a series of layers which vary in velocity from about 8.4 to 3.6 km/sec from the surface into the mantle over a scale of about 1 km are needed to explain the data. Clearly, this is geologically unreasonable.

An immediate conclusion is that other mechanisms of scattering are needed over and above body wave scattering in plane layers. It is likely that there is significant body wave to surface wave scattering in near surface layers (Dainty et al, 1974; Aki and Chouet, 1975; Dainty and Toksoz, 1977). This is expected because of the heterogeneous geology. It is also clear that 2 and 3D structures are required in the area to produce the large tangential particle motions observed in the data. Numerical experiments with 2D elastic finite difference methods show that, for an equal amplitude scattered field, velocity variations in two dimensions are about half that needed for velocity variations in one dimension(McLaughlin et al, 1985). Thus, assumption of simple 1D body wave scattering for explaining much of the receiver function coda at this station is naive.

Energy Flux Models for Plane Wave Scattering

The plane layered model simulations are instructive in showing deficiencies in basic modeling assumptions when treating the receiver function data. However, it would also be useful if the coda data could be parameterized in such a way to guide the analysis. For example, are there aspects of the coda decay which preclude reasonable plane layered models in other situations? Also, what does the amplitude of the coda suggest about the magnitude of scattering near a receiver?

Teleseismic P wave coda has been the subject of a number of studies (e.g., Aki, 1973; Dainty and Toksoz, 1977; McLaughlin et al, 1983; Levander and Hill, 1985; Frankel and Clayton, 1986; Cessaro and Butler, 1987). These studies are closely

related to general problems in coda generation due to lithospheric structure in local and regional data sets (e.g., Aki, 1969; 1980; Aki and Chouet, 1975; Dainty and Toksöz, 1977; Gao et al, 1983; Richards and Menke, 1983; Gupta and Blandford, 1983; Wu and Aki, 1985a,b; Cessaro and Butler, 1987; Frankel and Wennerberg, 1987, Vidale and Helmberger, 1988).

A number of techniques are available to parameterize the coda level and time decay based on the Born approximation of weak single scattering or of diffusion of coda energy for extreme scattering (e.g., Aki and Chouet, 1975; Aki, 1980; Dainty et al, 1974). Recent work has concentrated on simulation studies using finite difference acoustic and elastic wave propagation methods(Levander and Hill, 1985; Frankel and Clayton, 1986) which implicitely include the entire scattered field. Levander and Hill(1985) examined scattering characteristics of a rough boundary between a surface layer and underlying halfspace and showed that much of the scattered field is dominated by Rayleigh wave propagation. Frankel and Clayton (1986) and McLaughlin et al (1985) examined P-SV propagation in 2D random media to examine scattering of high frequency (f>1hz) seismic waves. Subsequently, Frankel and Wennerberg(1987) developed a simple theory based on previous finite difference simulations to parameterize coda levels, scattering attenuation, and intrinsic attenuation for 2 and 3D scalar wave fields.

The success of a number of receiver function studies in determining plane layered crustal and upper mantle structure indicates that the scattered wave field may be thought of being composed of a "coherent" contribution from Ps conversions and reverberations from discrete interfaces and a "stochastic" contribution from smaller scale heterogeneities. The coherent field can be seen over a large solid angle of ray paths. The stochastic field changes quickly with ray parameter and ray azimuth. Examples of the stochastic field are variation in tangential P wave first motions over the events of the 235^{0} stack in Figure 3b as well as coda arrivals with long lapse times from the first arrival. The

success of any deterministic receiver function study depends critically on the coherent field being dominant. However, the incoherent field, which is usually ignored in such studies, also contains statistical information on the degree of heterogeneity in the structure which may be very useful.

Past studies have not entirely addressed energy partitioning and the numerous scattering mechanisms that may be affecting formation of the full scattered field even for plane wave propagation. This problem is difficult since solutions of the wave equation for 2 and 3D complex structure must be examined. A heuristic approach will be used here to develop an operational theory appropriate to the three component receiver data. The purpose of doing this is to empirically compare coda levels and decay between different receivers for classification purposes and to suggest avenues of research that will address the actual wave propagation problems. This heuristic approach will also be used to quantify the differences between 1D structure coda development and coda observed in the data.

A useful method of parameterizing the P coda can be derived following Frankel and Wennerberg(1987). They examined scalar 2D finite difference simulations and suggested that scattered energy behind a cylindrical or spherical wavefront distributes itself uniformly over the volume behind the wavefront. Aki and Chouet (1975) arrived at the same conclusion when examining coda of regional earthquakes. This simple assumption yielded useful formulae for coda level and decay in cases of strong multiple scattering as well as the limiting case of weak single scattering. Theory for an energy flux model with plane wave propagation in a wholespace will be developed since simple wholespace models are widely used in many coda studies. It is also useful to examine a simple wave propagation regime to motivate more realistic scattering models.

Consider first a source of plane waves which radiates two oppositely propagating plane waves in a scattering wholespace. The total instantaneous

energy or power, E_T is given by the sum of the direct wave power, E_D, and the coda power, E_C.

$$E_T = E_D + E_C \quad . \tag{1}$$

Specify that

$$E_D = E_T e^{-\omega t/Q_s} \tag{2}$$

where t is time, ω is circular frequency and Q_s is the quality factor for attenuation due to wave scattering. Substitution of (2) into (1) gives

$$E_C = E_T (1 - e^{-\omega t/Q_s}) \quad . \tag{3}$$

Coda amplitude, A_c, is related to the coda power density, ξ_C, through the principal assumption that the coda energy distributes itself uniformly behind the two propagating plane waves. First we have

$$A_C = d \sqrt{\xi_C} \tag{4}$$

d is a scaling factor. For P and S plane waves $d = 1/\sqrt{\rho}$ where ρ is density. If δS is the unit plane wave area, r the propagation distance from source to receiver and α P-wave velocity, then the coda power density is

$$\xi_C = \frac{E_C}{\text{Volume}} = \frac{E_C}{2\, r\, \delta S} = \frac{E_C}{2\, \alpha\, t\, \delta S} \quad . \tag{5}$$

Using (3), (4) and (5) we obtain

$$A_C = \frac{d\sqrt{E_T}}{\sqrt{2\alpha t}} \frac{(1 - e^{-\omega t/Q_s})^{\frac{1}{2}}}{\sqrt{dS}} \quad . \tag{6}$$

E_T can be estimated using the observed direct wave amplitude and correcting it for attenuation through the scattering medium. Thus,

$$E_T = 2 E_D' e^{+\omega t_d/Q_s} \tag{7}$$

where E_D' is the observed direct wave power and $t_d = r/\alpha$. The factor of two comes from the fact that two plane waves are propagating in the medium and contribute to the scattered field. Plane wave propagation theory is used to obtain the estimate of direct wave power. First consider the integral of the square of the ground velocity, A(t),

$$I_D = \int_{t_1}^{t_2} A^2(t)\, dt \quad . \tag{8}$$

Times t_1 and t_2 bound the direct wave arrival and are estimated from the data. The direct wave power is therefore

$$d^2 E_D' = \alpha I_D\, dS \quad . \tag{9}$$

Substitution of (9) into (7) and of (7) into (6) gives

$$A_C = \frac{\sqrt{I_D}}{\sqrt{t}} e^{+\omega t_d/2Q_s} (1 - e^{-\omega t/Q_s})^{\frac{1}{2}} \quad . \tag{10}$$

As Frankel and Wennerberg (1987) show, the effect of attenuation due to scattering determines the initial level of the coda scattered from the direct

wave but coda decay with time is mainly controlled by the time-dependent increase in volume behind the wavefront. In this plane wave case, the $1 / \sqrt{t}$ dependence is due the linearly increasing volume between the two oppositely propagating plane waves.

Relation (1) is useful for describing the coda for a plane wave propagating in a thick layer where coda lapse times (wave arrive time relative to the direct wave) are less than the arrival time of waves which interact with the lower boundary of the layer assuming the observation point is at the surface. This corresponds to lapse times of less than 5 seconds for receivers on typical continental crust. A more appropriate model for receiver function coda is scattering in a heterogeneous layer overlying a homogeneous, isotropic halfspace. In this situation, a vertically propagating plane wave sweeps through the layer once on its way to the receiver, reflects from the free surface and sweeps through yet another time on its way back to the halfspace. Energy is scattered from the plane wave into coda energy.

A variation of this problem was studied by Dainty et al(1974) and Dainty and Toksoz(1977) where they assumed that scattering in the layer followed solutions to the diffusion equation. Also assuming that all energy within the layer was scattered energy they obtained the following analytic solution for the scattered energy field at the free surface, m(t) (assuming no intrinsic attenuation):

$$m(t) = \frac{4}{h} \sum_{n=1}^{\infty} \frac{a_n \cos a_n}{2 a_n + \sin 2 a_n} e^{-\frac{t \xi_v a_n^2}{4 h^2}} \quad . \qquad (11)$$

h is layer thickness and ξ_v is the vertical diffusivity of energy through the boundary of the layer into the halfspace. The coefficients, a_n, are found as solutions of the following equation:

$$a_n \tan a_n = \frac{4hv}{\xi_v} \qquad (12)$$

where v is the seismic velocity of the halfspace.

The dominant term of (11) for long lapse times and a high vertical diffusion rate can be shown to be for n=1. Thus, for cases where diffusion of scattered energy occurs quickly, coda energy decays like

$$m(t) \propto e^{-\gamma t} \qquad (13)$$

where $\gamma = \xi_v a_1^2 / 4h^2$. This behavior can be incorporated into a hybrid model containing aspects of plane wave propagation in a layer with assumption of homogeneity of the scattered field within the layer.

Consider a horizontal scattering layer of thickness h overlying a homogeneous and isotropic halfspace. A vertically propagating plane wave is incident from below, passes through the layer, reflects from the free surface and passes back through the layer into the halfspace. The total power in the system can be written as

$$E_T = E_D + E_C + E_O \qquad (14)$$

where a new term E_O has been introduced to describe the amount of instantaneous energy which diffuses out the bottom of the layer at the expense of the coda instantaneous energy, E_C. Based on the behavior of (11) above, we assume that

$$\frac{dE_O}{dt} = \gamma E_C \qquad (15)$$

which by simple integration yields

$$E_C = E_C (e^{\gamma t} - 1) \tag{16}$$

where it is specified that E_o=0 at t=0. As before, the power in the direct wave after interacting with the layer is

$$E_D = E_T e^{-\omega 2 t_d / Q_s} \tag{17}$$

where the factor of two in the exponent comes from the wave passing twice through the layer. Obviously, (14) is appropriate for short-duration direct waves and times greater than $2t_d$.

Substituting (17) and (16) into (14) gives

$$E_C = E_T \left(1 - e^{-\omega 2 t_d / Q_s} \right) e^{-\gamma t} \quad . \tag{18}$$

Also recognizing the volume swept by the plane wave is now $h\,\delta S$, the coda power density becomes

$$\xi_C = \frac{E_C}{\alpha\, t_d\, \delta S} \quad . \tag{19}$$

As before, the total instantaneous energy available to the system can be estimated from the observed direct wave power, E_D', by

$$E_T = E_D' e^{+\omega t_d / Q_s} \tag{20}$$

and using (9) gives

$$A_c = \frac{\sqrt{t_c}}{\sqrt{t_d}} e^{+\omega t_d/2Q_s} \left(1 - e^{-\omega t_d/Q_s}\right) e^{-\gamma t_c} \quad . \qquad (21)$$

Note that this form for coda amplitude looks superficially the same as that in (10) except for the exponential factor of time in the numerator of (21). Indeed, the time decay of the coda is controlled entirely by this factor. If $\gamma = 0$ is assumed so that no coda energy can diffuse out of the layer, then the coda level is constant for all time, consistent with the plane wave assumption of a packet of energy being homogeneously dispersed throughout the layer. Thus, the decay of the coda field is functionally equivalent to the leading term for the formal solution (11) and (13) particularly considering that energy is proportional to the square of amplitude.

Anelastic attenuation can be included in relations (10) and (21) as the factor

$$e^{+\omega t_d/2Q_I} e^{-\omega t/2Q_I} \qquad (22)$$

where Q_I is the intrinsic attenuation of the medium. The first exponential in (22) is the correction factor to determine total energy from the direct wave and the second exponential gives the attenuation of coda amplitude. Note that the effect of coda energy diffusing out of the layer given in (21) is exactly the same as intrinsic attenuation. We would therefore expect that it would be very difficult to impossible to separate the two effects in practice using the teleseismic coda data.

An implicit assumption in developing (10) or (21) is that the scattered field is of the same wave type as the primary. These equations are appropriate for, say, the scattered pressure field from an incident P wave. Even for simple 1D layered structures, much of the scattered field is composed of P-to-S conversions. For 2D and 3D structures, there is evidence that much of the

scattered field seen at the surface is composed of low group-velocity surface waves (Dainty et al 1974; Aki and Chouet, 1975; Levander and Hill, 1985). Thus, there is a procedural problem of relating observed coda wave amplitude to energy since the wave type contained in the coda must be known before hand. In principle, it is possible to directly infer the energy contained in a wavefield if strain observations are available. However, three-component displacement data cannot be used without assumptions on wavetype.

Recognizing these limitations, we nevertheless use equations (10) and (21) as guides to the analysis of the three-component data. These equations will be useful in parameterizing relative levels of coda and coda decay between isolated recievers but are clearly deficient in addressing all of the scattering mechanisms which are probably important in teleseismic coda development.

Some operational aspects of examining coda decay are patterned after previous studies (e.g., Richards and Menke, 1983; Frankel and Wennerberg, 1987). Observed three-component data for a single event are first narrow band-pass filtered with a Butterworth recursive filter in the forward and backward directions. The two-pole filter used had corner frequencies of 0.25 and 1 hz so the following results are appropriate for 0.5 hz waves. Once the data were filtered the intensity of the direct P wave at 0.5 hz was estimated by squaring the signal, choosing t_1 and t_2 (equation 8) from the duration of large motions on the vertical component and integrating over this time interval. The power of the direct wave was estimated using all three components of motion over the time interval inferred from the vertical component. The integral of the squared velocity used for equations (10) or (21) was the square root of the sum of the squares of the integrals from each component of ground motion. Each component was then scaled by dividing the square root of this total squared velocity integral. The envelope of each component was then computed by forming the analytic signal (Farnbach, 1975) and taking its modulus. The total coda time

series for one event was then found by summing the squares of the envelopes of the three components at each time point and taking the square root of the sum. Resulting coda envelopes for separate events were then averaged to obtain a better estimate of coda level.

Figure 11 shows the results of this process using four deep earthquakes recorded at PAS (Table 1). Deep events were chosen to avoid contamination by near-source scattering effects. The observed levels of coda are very high. Indeed, an examination of the raw data (e.g., Figure 2) shows that much of the coda comes from the horizontal components. Theoretical curves computed using equation (10) are superimposed on the coda decay curve in Figure 11 and show that an apparent scattering Q_S of 200 to 300 is required. The coda time decay appears to be very slow and is roughly consistent with $1/\sqrt{t}$ found in this model of scattering.

Figure 12 demonstrates, however, that the simple 1D simulations are not consistent with coda decay following equation (10). The coda curve for the "20%" model was constructed by stacking 10 vertical and horizontal component realizations (20 time series in all) of models which had a velocity standard deviation of 20% and a layer thickness of 60 km. The "10%" curve was obtained by stacking 9 vertical and horizontal component realizations (18 time series) for models which had a velocity standard deviation of 10% and a layer thickness of 30 km. The observed coda decay is linear on the logarithm plot and falls off much faster than implied by (10). The linear fall-off is consistent with the scattering layer-over-halfspace model where coda energy diffuses out of the layer into the halfspace governed by equation (15). The 1D simulations included no effect of anelastic attenuation.

Figure 12 also shows least-squares linear fits to the coda decay to obtain Q_S and γ in equation (21). The slope of the log-coda curve yields γ and the zero time intercept can be used to directly solve for Q_S. The standard

deviation of the least-squares fit was also used to estimate allowable Q_S variation by adding and subtracting the standard deviation from the zero intercept time to find a lower and upper bound of Q_S, respectively. These values are displayed Table 3. Coda from the simulations show that the diffusing layer model correctly predicts the form of coda decay although the model does not formally treat the scattering mechanism of P to S conversions within the layer. The decay rate is very sensitive to the velocity standard deviation but Q_S estimates are surprisingly the same, within the error of determination.

It is interesting to compare results for PAS with those from another station to get an appreciation for the level of scattering implied by the data. Three deep events recorded on the broad-band DWWSSN system at SCP (State College, PA) were analyzed in the same way. Event parameters can be found in Table 4 and the data are displayed in Figure 13. The Benioff 1-90 and intermediate-period DWWSSN systems are sufficiently similar for the purposes of this comparison, particularly since the same band-pass filter was used on the data.

Figure 14 compares the coda decay curves for PAS and SCP. Structure under SCP is seen to be simplier than that at PAS (Langston and Isaacs, 1981; Ammon, 1988 personal communication) and gives rise to lower amplitude Ps conversions as well as coda. Coda decay for SCP is twice as fast than that observed for PAS (Table 3). Q_S is found to be lower for PAS with use of equation (21) giving a value of 239 compared to 582 for SCP.

Discussion

The scattering layer-over-halfspace model reproduces the principal behavior of the 1D structure simulations (Figure 12) and is consistent with coda decay in the PAS and SCP data. The simple assumptions of homogeneity of the coda field and diffusion of energy into the halfspace seem to describe the basic mechanisms

of coda formation and is consistent with previous observations of the behavior of data and 2D simulation studies

Aki and Chouet(1975) estimated the diffusivity of the lithosphere in Japan and California using a diffusion model of coda formation applied to local earthquake data. They found high diffusion rates having the effect of homogenizing the coda field behind the wavefront. Frankel and Wennerberg(1987) took these ideas further by examining the coda field in finite difference simulations and constructing a simple energy flux theory to explain the formation coda. Although the assumptions of homogeneous coda and diffusive energy flow across the layer boundary are reasonable, the actual mechanisms of coda formation are not directly addressed in an equation like (21) which leads to the problem of estimating coda energy from an unknown wavefield.

Much of the coda in the 1D simulations is a product of P to S conversions and reverberations. The energy scattered into S waves is obviously a function of ray parameter. As the direct wave incidence angle increases, more P to S conversions will occur. This can be verified directly by calculation but can be easily seen in the behaviour of the conversion coefficient at a boundary. Thus, it can be expected that coda fall-off and levels will change for waves of different incidence angle if 1D structure is appropriate. P to S scattering in 2D structures is more complex (Frankel and Clayton, 1986; McLaughlin et al 1985) but appears to become less sensitive to incidence angle. P and S to Rayleigh scattering is probably a major component of the coda field at relatively low frequencies (<1hz) (Aki and Chouet,1975). These scattering mechanisms may control the coda formation in the data presented here. In terms of the application of equation (21) the problem amounts to estimating $\underline{d}$, the scaling factor relating energy density to wave amplitude in equation (4). Even for 1D structure $\underline{d}$ depends on incidence angle and includes the free surface receiver functions (e.g., Helmberger, 1968). It is of some interest to examine the energy partitioning in

the coda of the simulations and, making some simple assumptions, the partitioning seen in the data.

As an approximation, consider the coda power being composed of S-wave, E_{C_S}, and P-wave, E_{C_P}, powers

$$E_C = E_{C_S} + E_{C_P} \quad . \tag{23}$$

Also define the energy partitioning coefficient by

$$\Gamma = \frac{E_{C_S}}{E_{C_P}} \quad . \tag{24}$$

For plane wave propagation

$$\left.\begin{aligned} E_{C_S} &= \rho \beta I_S \\ E_{C_P} &= \rho \alpha I_P \end{aligned}\right\} \tag{25}$$

where I_S and I_P are the estimated integrals of squared velocity for S-wave and P-wave motions, respectively. The S-wave velocity is given by β. For 1D structure models and for incident P waves of small incidence angle, S-waves occur primarily on the horizontal component and P on the vertical. The respective wave integrals can therefore be directly estimated using equation (8) by performing the integration over the filtered and squared waveform from the end of the direct wave arrival to some reference time in the coda. This was done for the waveforms obtained from the 10% and 20% 1D simulation models. Both models give similar results where, for the ray parameter considered (0.06 sec/km) in constructing the synthetics, roughly 70% of the scattered energy occurs as S-wave energy (A value of 0.7 ± 0.3 was obtained for both simulations using the individual waveforms of each model realization.) Changing the ray parameter to 0.04 sec/km, appropriate for source distances of 85^{o} reduces the S-wave energy

to 50% and less for the synthetics. The free surface effect is assumed to be the same for both P and S for these low angles of incidence.

Small differences in correcting the data for wave propagation effects are of little consequence to this discussion since wave types in the observed coda data are largely unknown. We treat the observed data in the same way where the S- and P-wave integrals are defined as:

$$\left.\begin{aligned} I_S &= \sqrt{I_{C_N}^2 + I_{C_E}^2} \\ I_P &= I_{C_Z} \end{aligned}\right\} \qquad (26)$$

where the subscripts Z, N, and E denote the component of ground motion. Assuming only S and P-wave partitioning in the PAS data yields a partitioning coefficient of 1.7 ± 0.4, a factor of 2 to 3 greater than expected compared to the 1D simulations. This result is consistent with the coda being comprised of low group-velocity surface waves scattered from incident P and S waves. Instantaneous energy will be proportional to the group velocity so that assuming a higher S velocity in (26) will cause the energy to be overestimated. These observations are consistent with observations of the coda at arrays (Aki, 1973; Aki and Chouet, 1975) and from theoretical wave propagation calculations (e.g., Levander and Hill, 1985). Powell and Meltzer (1984) also found direct evidence for a high level of scattering under southern California in their study of coherency across the SCARLET array.

It thus appears that coda level and coda decay at PAS is inconsistent with plausible 1D earth models. The observed data show slow coda decay implying a relatively long dwell time of coda energy in the crust as well as high amplitudes. The high amplitudes are consistent with the coda field being primarily composed of scattered surface waves. Even the coda decay seen at SCP implies unreasonable 1D structure since the data imply virtually the same attenuation and decay as the 20% velocity model (Table 3).

These aspects of the receiver function data can be routinely quantified in other data sets to motivate an interpretation of structure under a receiver. If the receiver function coda data show tendencies that are inconsistent with simple 1D models then inversion of selected phases at long lapse times (>10 sec) from the first arrival or inversion of the entire waveform becomes suspect. This result is not surprising when one simply looks at the anomalies contained within the data but the theoretical treatment presented here can help quantify both the gross characteristics of the observed data and the justification of a particular modeling strategy.

The large size of the initial inferred Ps conversion with anomalous particle motion implies the existence of an interface which dips to the north under the San Gabriel Mountains with a gentle dip of 10^{0} or less. The large relative amplitude, seen also on long-period data, implies an S-wave velocity contrast greater than 1 km/sec. It is conceivable that focussing due to a curved interface accentuates the Ps conversion relative to direct P. However, it is difficult to produce such effects unless the interface radius of curvature is comparable to the depth of the interface (Lee, 1983) so that a caustic is formed at the surface.

The northward dip of the interface suggests that it is a major structure associated with the southward overthrusting of the San Gabriel Mountains. If the amplitude of the conversion is due to large velocity contrasts, then a low velocity zone is required at mid to deep crustal levels. It is interesting to note that this low velocity zone occurs just under the seismogenic zone of the region and may be the seismic signature of the decoupling zone of upper crustal and lower crustal-upper mantle microplates (Humphries, 1984).

Conclusions

The receiver function data set for PAS suggests the scattering is occuring in a highly heterogeneous crust. Broad-band Benioff 1-90 data from teleseisms show anomalous tangential particle motions and a high amplitude coda which decays slowly. Initial portions of the radial and tangential receiver functions show a coherent inferred Ps conversion which displays a polarization anomaly of 45^{0} for most data. Using the amplitude, polarity, and timing of this phase seen in stacks of the data and from a direct observation in an incident PKIKP phase, a high S-wave velocity contrast (>1 km/sec) interface is inferred at approximately 20 km depth. The interface dips less that 10^{0} to the north and appears to be a major structure associated with southward overthrusting of the San Gabriel Mountains.

Observed coda level and decay was examined using two methods. One was direct simulation of 1D stochastic structures. Plane wave synthetic seismograms were computed for random plane layered models with an exponential correlation function and with 10% and 20% standard deviations in velocity. The PAS data showed larger scattering effects than the simulations indicating that geologically unreasonable 1D models are required to explain the coda data. The 1D models also are obviously deficient in explaining the degree of off-azimuth scattering seen in the data.

The other method consisted of examining coda behavior using an energy flux model developed for a scalar plane wave incident on a scattering layer over a homogeneous halfspace. A scattering layer model was considered since it is likely that major velocity perturbations are largely confined to the crust. Two fundamental assumptions were made to develop the model and were based on previous empirical observations of the behavior of earthquake coda and numerical experiments. It was assumed that the coda field distributes itself homogeneously within the layer and that coda energy diffuses across the layer-

halfspace boundary. Coda decay is seen to be controlled entirely by the diffusion constant of energy flow across the layer boundary. Synthetic seismograms from the 1D simulations show that the simple energy flux model explains the form of coda decay. One implication of this model is that the diffusion effect is indistinguishable from anelastic attenuation. Thus, it is likely that teleseismic coda data cannot be used to estimate local anelastic attenuation.

PAS and SCP data from selected deep earthquakes were analyzed using this model and it was found that PAS had a lower scattering Q_S (~239) compared to SCP (~582) and that the coda decay for SCP was twice as fast as that for PAS. The absolute values of scattering Q_S obtained with the model are subject to assumptions on the types of waves contained with the wavefield and probably represent lower bounds to the actual Q values. The comparison between the two stations shows that scattering is lower in a tectonically quiescent area with less variable geology as expected.

An analysis of energy in the horizontal and vertical components of the 1D synthetics and the PAS data suggests that much of the energy contained in the observed coda is from scattered surface waves.

Finally, the observational techniques proposed here can be used to justify or not justify the use of 1D plane layered inversion models or the analysis of isolated phases late in the coda of receiver function data. The PAS data are clearly inconsistent with geologically plausible 1D models as are the SCP data. Further research is needed to quantify the nature of 2 and 3D scattering in causing teleseismic coda and in quantifying the application of simple energy flux models as developed here.

Acknowledgements

This research progressed from a study of the same data by J.J. Lee. He is gratefully acknowledged in collecting much of the PAS data and contributing as a colleague to the understanding and limitations of dynamic ray tracing to the receiver function problem. The personel at the Seismological Laboratory at Caltech are also acknowledged for their help in collecting the data for this study. Hiroo Kanamori provided information on instrument calibration and is gratefully acknowledged. Hye-Sun Kim helped digitize much of the data seen here and Terry Ott also helped with data processing. I would also like to thank Chuck Ammon for dearchiving the SCP waveforms and contributing his comments on the paper. John Louie and Roy Greenfield also provided useful comments and interesting discussions on these topics. Early parts of this research were supported by the National Science Foundation under Grant EAR-8013704. This research was also sponsored by the Defense Advanced Research Projects Agency through the Air Force Geophysics Laboratory under contract #F19628-87-K-0024.

References

Aki, K., Analysis of seismic coda of local eathquakes as scattered waves, Jour. Geophys. Res., 74, 615-631, 1969.

Aki, K., Scattering of P waves under the Montana LASA, Jour. Geophys. Res., 78, 1334-1346, 1973.

Aki, K., Scattering and attenuation of shear waves in the lithosphere, Jour. Geophys. Res., 85, 6496-6504, 1980.

Aki, K., and B. Chouet, Origin of coda waves: source, attenuation, and scattering effects,Jour. Geophys. Res., 80, 3322-3342, 1975.

Burdick, L.J., and C.A. Langston, Modeling crustal structure through the use of converted phases in teleseismic body waveforms, Bull. Seism. Soc. Am., 67, 677-692, 1977.

Cessaro, R.K., and R. Butler, Observations of transverse energy for P waves recorded on a deep-ocean borehole seismometer located in the northwest Pacific, Bull. Seis. Soc. Am., 77, 2163-2180, 1987.

Dainty, A.M., M.N. Toksoz, K.R. Anderson, P.J. Pines, Y. Nakamura, and G. Latham, Seismic scattering and shallow structure of the Moon in Oceanus Procellarum, The Moon, 9, 11-29, 1974.

Dainty, A.M., and M.N. Toksoz, Elastic wave propagation in a highly scattering medium - a diffusion approach, Jour. Geophysics, 43, 375-388, 1977.

Farnbach, J.S., The complex envelope in seismic signal analysis, Bull. Seism. Soc. Am., 65, 951-962, 1975.

Frankel, A., and Clayton, R.W., Finite difference simulations of seismic scattering: implications for the propagation of short-period seismic waves in the crust and models of crustal heterogeneity: Jour. Geophys. Res., 91, 6465-6489, 1986.

Frankel, A., and L. Wennerberg, Energy-flux model of seismic coda: separation of scattering and intrinsic attenuation, Bull. Seismol. Soc. Am., 77, 1223-1251, 1987

Gao, L.S., L.C. Lee, N.N. Biswas, and K. Aki, Comparison of the effects between single and multiple scattering on coda waves for local earthquakes, Bull. Seism. Soc. Am., 73, 377-389, 1983.

Gupta, I.N., and R.R. Blandford, A mechanism for generation of short-period transverse motion from explosions, Bull. Seism. Soc. Am., 73, 571-591, 1983.

Hadley, D., and H. Kanamori, Seismic structure of the Transverse Ranges, California: Bull. Geol. Soc. Am., 88, 1469-1478, 1977.

Hagiwara, T., A note on the theory of the electromagnetic seismograph, Bull. Earthquake Res. Inst., 36, 139-164, 1958.

Haskell, N.A., Crustal reflection of plane P and SV waves, Jour. Geophys. Res., 67, 4751-4767, 1962.

Hearn, T.M., and R.W. Clayton, Lateral velocity variations in southern California. I. Results for the upper crust from Pg waves: Bull. Seismol. Soc. Am., 76, 495-509, 1986a.

Hearn, T.M., and R.W. Clayton, Lateral velocity variations in southern California. II. Results for the lower crust from Pn waves: Bull. Seismol. Soc. Am., 76, 511-520, 1986b.

Hebert, L. and C.A. Langston, Crustal thickness estimate at AAE (Addis-Ababa, Ethiopia) and NAI (Nairobi, Kenya) using teleseismic P-wave conversions, Tectonophysics, 111, 299-327, 1985.

Helmberger, D.V., The crust-mantle transition in the Bering Sea, Bull. Seism. Soc. Am., 58, 179-214, 1968.

Humphreys, E., R.W. Clayton, and B. Hager, A tomographic image of mantle structure beneath southern California: Geophys. Res. Lett., 11, 625-627, 1984.

Langston, C.A., The effect of planar dipping structure on source and receiver responses for constant ray parameter, Bull. Seism. Soc. Am., 67, 1029-1050, 1977.

Langston, C.A., Structure under Mount Rainier, Washington, inferred from teleseismic body waves, Jour. Geophys. Res., 84, 4749-4762, 1979.

Langston, C.A., and C.M. Isaacs, A crustal thickness constraint for central Pennsylvania, Earthquake Notes, 52, 13-22, 1981.

Lee, J.-J., A three-dimensional ray method and its application to the study of wave propagation in crustal structure with curved layers, Ph.D. Thesis, Pennsylvania State University, University Park, PA, 1983.

Lee, J.-J., and C.A. Langston, Three-dimensional ray tracing and the method of principal curvature for geometric spreading, Bull. Seism. Soc. Am., 73, 765-780, 1983a.

Lee, J.-J., and C.A. Langston, Wave propagation in a three-dimensional circular basin, Bull. Seism. Soc. Am., 73, 1637-1653, 1983b.

Levander, A.R., and N.R. Hill, P-SV resonances in irregular low-velocity surface layers, Bull. Seism. Soc. Am., 75, 847-864, 1985.

McLaughlin, K.L., L.M. Anderson, and Z.A. Der, Investigation of scattering and attenuation of seismic waves using 2-dimensional finite difference calculations in Multiple Scattering of Waves in Random Media and Random Rough Surfaces, The Pennsylvania State University, University Park, PA, 1985.

Owens, T.J., Determination of crustal and upper mantle structure from analysis of broadband teleseismic P-waveforms, Ph.D. Thesis, The University of Utah, Salt Lake City, 1984.

Owens, T.J., G. Zandt, and S.R. Taylor, Seismic evidence for an ancient rift beneath the Cumberland Plateau, TN: a detailed analysis of broadband teleseismic P-waveforms, Jour. Geophys. Res., 89, 7783-7795, 1984.

Owens, T.J., S.R. Taylor, and G. Zandt, Crustal structure at regional seismic test network stations determined from inversion of broadband teleseismic P waveforms, Bull. Seis. Soc. Am., 77, 631-662, 1987.

Powell, C.A. and A.S. Meltzer, Scattering of P-waves beneath SCARLET in southern

California, Geophys. Res. Lett., 11, 481-484, 1984.

Richards, P.G., and W. Menke, The apparent attenuation of a scattering medium, Bull. Seism. Soc. Am., 73, 1005-1021, 1983.

Vidale, J.E., and D.V. Helmberger, Elastic finite-difference modeling of the 1971 San Fernando, California, earthquake, Bull. Seismol. Soc. Am., 78, 122-141, 1988.

Wu, R.S., and K. Aki, Scattering characteristics of elastic waves by an elastic heterogeneity, Geophysics, 50, 582-595, 1985a.

Wu, R.S., and K. Aki, Elastic wave scattering by a random medium and the small-scale inhomogeneities in the lithosphere: Jour. Geophys. Res., 90, 10261-10273, 1985b.

Yerkes, R.F., T.H. McCulloh, J.E. Schoellhamer, and J.G. Vedder, Geology of the Los Angeles Basin Area, California - An Introduction, U.S.G.S. Prof. Paper 420-A, 1-47, 1965.

Appendix

Nominal instrument constants for the Benioff 1-90 system are pendulum period of 1 sec, galvenometer period of 90 sec, damping constants of 1 for both the seismometer and gal ometer, a coupling constant of 0.05, and magnification of 3000 (H. Kanamori, personal communication 1987). A calibration of the system was started in 1962 but was never totally completed. Calibration of the vertical component showed a peak magnification of 2700, 10% under nominal specifications. Experience with the system suggests that instrument constants are good to about 30%. Because calibration of the instruments can affect the results of rotation of the data and the source equalization, it is of some interest to examine the results of errors in the instrument constants. It will be assumed that the receiver response is ideal consisting of motions confined to the sagittal plane containing the ray. Vector rotation of the horizontal displacement components to obtain radial and tangential ground motions follows

$$\left.\begin{aligned} u_R(t) &= -u_N(t)\cos(\theta) - u_E(t)\sin(\theta) \\ u_T(t) &= u_N(t)\sin(\theta) - u_E(t)\cos(\theta) \end{aligned}\right\} \qquad \text{(A1)}$$

where the subscripts R and T denote radial and tangential motions, respectively, and the subscripts N and E denote north-south and east-west motions, respectively. θ is the backazimuth angle to the source from the receiver. If the respective instrument responses are given by $i_n(t)$ and $i_e(t)$, and R(t) is a common radial response for plane layered structure, then

$$\left.\begin{aligned} u_R(t) &= R(t) * \{ i_n(t)\cos^2\theta + i_e(t)\sin^2\theta \} \\ u_T(t) &= R(t) * \{ i_e(t) - i_n(t) \}\sin 2\theta/2 \end{aligned}\right\} . \qquad \text{(A2)}$$

The largest errors in rotation occur when $\theta = 45^{o}$ which gives

$$\left.\begin{aligned} u_R(t) &= \tfrac{1}{2} R(t) * \{ i_n(t) + i_e(t) \} \\ u_T(t) &= \tfrac{1}{2} R(t) * \{ i_e(t) - i_n(t) \} \end{aligned}\right\} \quad . \qquad (A3)$$

Tangential motion, in this case, is caused by differences in the instrument responses of the two components. Clearly, if small differences occur in the responses then the radial motions will be little affected since the net response will the average of the two. If magnifaction is known to within some factor ϵ such that

$$\left.\begin{aligned} i_n(t) &= (1 \pm \epsilon) \, i(t) \\ i_e(t) &= (1 \pm \epsilon) \, i(t) \end{aligned}\right\} \qquad (A4)$$

where i(t) is the nominal response then, assuming a backazimuth of 45^{o},

$$\left.\begin{aligned} u_R(t) &= R(t) * i(t) \{ 1 \pm \epsilon \} \\ u_T(t) &= R(t) * i(t) \{ \pm \epsilon \} \end{aligned}\right\} \quad . \qquad (A5)$$

Thus, the tangential component, in the worst case, will approximately be 30% of the radial component if magnification is only known to 30% and will look identical to the radial component in waveshape. The data for PAS (Figure 2) show extreme differences in waveshape between the horizontal components which cannot be due to magnification errors.

The equations for electromagnetic seismographs (Hagiwara, 1958) were used to estimate the difference in instrument responses if 30% variations in the instrument constants are assumed. Figure A1 displays the results for amplitude spectra. 30% changes in the galvonometer period and damping, and the seismometer period and damping were assumed relative to the nominal response. Theoretical responses were calculated in the frequency domain and inverse Fourier transformed to obtain impulse responses. Using equation (A3) as a guide, the

perturbed responses were then subtracted from the nominal response and then Fourier transformed to obtain the amplitude spectrum. Thus, the four curves below the nominal 1-90 response seen in Figure A1 are the amplitude spectra of the differenced impulse responses. They can be considered numerical derivatives of the instrument response if divided by 0.3. According to equation (A2), these curves would also be the spectra of the tangential impulse response.

A change in the galvonometer period or damping results in a response 2 to 3 orders of magnitude lower than the nominal response in the band centered about 1 hz (Figure A1). Thus, it is not likely that errors in these parameters will be of any consequence in the data. Changes of 30% in seismometer period produces a tangential impulse response about a factor of 4 lower than the nominal response and looks nearly identical to the nominal response. A change in seismometer period appears as a change in magnification. The tangential waveform would differ by only a constant compared to the radial waveform. A change in seismometer damping, however, has the greatest change in the shape of the spectrum. A 90^{o} phase shift is evident at 1 hz which, for band limited data, would make the tangential motion appear Hilbert transformed compared to radial motion. Fortunately, this response is 1 to 2 orders of magnitude lower than the nominal response. In summary, plausible changes in the instrument constants for the 1-90 system cannot explain the anomalous particle motions seen in the data.

It cannot be discounted that magnification errors may occur in the data. An empirical test was made by comparing the ratio of north-south, east-west, and vertical amplitudes of the first P pulse observed in the 1-90 data with that seen in the 30-90 data. P-wave data for the 12/28/73, 03/23/74, and 11/29/74 events were used. Considering that the pass-bands of the two instruments are different, amplitude ratios of the different ground motion components between instruments were within 20% of each other.

Finally, the data can be used in a the test proposed by Langston (1979) to

demonstrate that major off-azimuth arrivals occur on both horizontal components for events with different backazimuths. Figure A2 shows the first 10 seconds of the P waveforms for the 02/01/73 and 12/28/73 events (also see Figure 2). Polarities have been adjusted to make the waveform comparison clearer and the P-waves have been aligned in time. The arrow in the middle pair of plots shows the location of the large Ps conversion studied in the main body of the paper. It clearly occurs on the north-south component for the 02/01/73 event and on the east-west component of the 12/28/73 event. Likewise, the corresponding east-west and north-south components (right pair of waveforms) show similar waveforms between events without the major arrival. This comparison shows that both horizontal instruments behaved in a similar fashion for the same wave propagation effect.

Table 1 - Event Parameters for Pasadena Data

Origin Date	Time(UT)	Lat (Deg.)	Lon (Deg.)	Mb	Depth (km)	Dist. (Deg.)	BAZ (Deg.)	Stack Group	
03/17/66	15:50:33	21.1S	179.2W	6.2	639	79.9	236.1	235	
11/20/71	07:28:01	13.4S	179.9W	6.0	551	81.9	234.8	235	
02/01/73	05:14:20	22.7S	62.2W	6.1	229	77.6	128.4	128	*
12/28/73	05:31:06	23.9S	180.0E	6.3	549	82.3	234.5	235	*
03/23/74	14:28:35	23.9S	179.8E	6.1	535	82.5	234.6	235	*
10/20/74	04:12:29	17.9S	178.6W	6.0	602	77.4	238.1	235	
11/29/74	22:05:22	30.7N	138.3E	6.1	419	83.3	302.5	315	*
02/22/75	22:04:37	24.9S	179.1W	6.2	375	82.4	233.7	235	
06/29/75	10:37:41	38.8N	130.0E	6.2	560	83.9	313.2	315	
01/23/76	05:45:30	7.5S	119.9E	6.4	614	120.0	282.4	235	
12/12/76	01:08:50	28.0N	139.6E	5.9	491	83.9	299.7	315	
09/23/78	16:44:26	11.0S	167.2E	6.5	200	85.4	249.9	235	
04/24/79	01:56:14	20.8S	178.7W	6.0	450	79.4	236.0	235	
05/13/79	06:38:15	18.9N	145.3E	5.9	250	84.8	289.2	315	
05/21/79	22:32:58	15.2S	70.1W	6.0	208	67.1	128.8	128	
06/27/79	09:58:03	7.1N	82.0W	5.8	150	42.9	120.6	128	
08/16/79	21:42:44	41.8N	130.7E	6.1	588	81.5	315.2	315	
11/23/79	23:49:04	4.8N	76.2W	6.4	200	48.6	117.4	128	
12/11/80	18:26:26	21.3S	68.1W	6.1	100	72.9	131.6	128	

* - Used in coda analysis

Table 2 - Plane Layered Crustal Models

Layer	Vp (km/sec)	Vs (km/sec)	Density (gm/cc)	Thickness (km)
Hadley and Kanamori Model				
1	5.5	3.0	2.6	4.0
2	6.2	3.5	2.7	16.0
3	6.8	3.8	2.85	11.0
4	7.8	4.5	3.1	10.0
5	8.3	4.8	3.35	-
Low Velocity Zone Model				
1	5.5	3.0	2.6	4.
2	6.2	3.5	2.7	6.
3	6.5	3.75	2.7	5.
4	5.6	3.23	2.7	6.
5	6.6	3.81	2.8	2.
6	7.2	4.16	2.9	2.
7	7.4	4.27	2.95	2.
8	7.6	4.39	3.0	5.
9	8.0	4.62	3.2	6.
10	8.3	4.8	3.35	-

Table 3 - Q_S and γ Determinations for Coda Stacks

Coda Stack	Least-Squares Fit Intercept	Slope	Stand.Dev.	Q_S	γ	High Q	Low Q
[illegible] Simulation	-0.970	-0.050	0.079	544	0.229	784	380
[illegible] Simulation	-0.985	-0.0098	0.057	584	0.045	761	450
PAS Data	-0.789	-0.0047	0.075	239	0.022	337	169
SCP Data	-0.984	-0.0092	0.105	582	0.043	944	359

(Scattering Q determinations where found using equation (21) for a 30 km thick scattering layer with an average P velocity of 6 km/sec.)

Table 4 - Event Parameters for State College Data

Date	Origin Time(UT)	Lat. (Deg.)	Lon. (Deg.)	Mb	Depth (km)	Dist. (Deg.)	BAZ (Deg.)
12/21/83	12:14:18	28.2S	63.2W		602	70.0	166
08/08/85	16:35:58	6.1S	113.4E	5.7	596	144.0	341
08/12/85	04:36:43	7.0S	117.2E	5.6	599	143.8	334

Figure Captions

Figure 1: Sketch map of southern California showing the location of PAS station and major faults of the area.

Figure 2: Selected data from deep earthquakes (see Table 1) recorded on Benioff 1-90 instrumentation at PAS. Z, NS, and EW waveforms denote observed vertical, north-south, and east-west components. R and T waveforms are the result of rotating the observed horizontal components into the theoretical backazimuth of the ray. The distance and backazimuth angle are given, in order, in the parantheses to the right of each event's date. Note the time scale difference for event 01/23/76.

Figure 3: Stacks of source equalized radial (top) and tangential (bottom) data for the three azimuthal groups considered in the text. The average and $\pm$ one standard deviation waveforms are shown in each panel. P and Ps arrivals are annotated.

(A) 128 Degree group

(B) 235 Degree group

(C) 315 Degree group

Figure 4: Comparison of the stacked radial and tangential equalized waveforms for the three backazimuth groups. Note the azimuthal dependence of the Ps conversion on the radial components. The waveforms have been shifted in baseline for viewing purposes.

Figure 5: Particle motion plots for the 315 and 235 degree equalized waveforms. The waveform data are displayed above the radial (R or RADI) - Tangential (T or TANG) particle motions. Arrows are shown on the particle motion plots every 0.5 sec. Waveform data included within the brackets are plotted below. Maximum amplitude for each waveform is shown to right of the waveform. Note that the P waves in both cases are polarized in the expected ray direction but the inferred Ps conversions have a polarization

anomaly of 45 degrees.

Figure 6: Comparison of data from the 11/29/74 event recorded on 1-90 (bottom) and 30-90 instrumentation at PAS. The arrows show the location of the Ps conversion discussed in the text for both data sets. Note particularly the extreme amplitude of the Ps conversion relative to the first P arrival on both IPN and LPN components.

Figure 7: Particle motion plot of the horizontal data for the 01/23/76 event. Data included within the bracket are plotted below with arrows occurring every 0.5 seconds. The Ps conversion is polarized almost perfectly northward and indicates the direction of dip of the causitive interface.

Figure 8: Comparison of synthetic radial waveforms for the two models of Table 2 with the 235 degree radial waveform stack. The arrow for the H-K (Hadley-Kanamori model) waveform shows the location of the Ps conversion from the Moho. The arrow for the LVZ (Low Velocity Zone model) waveform shows the location of the Ps conversion produced at the base of the crustal low velocity zone. The baselines of the synthetic waveforms have been shifted for viewing purposes.

Figure 9: Velocity depth functions for the Hadley-Kanamori model and the LVZ model used in constructing the synthetic seismograms of Figure 8. Also shown are the stochastic 1D models used in the calculation of the synthetics displayed in Figure 10. Note that velocity and depth scales are different among the plots.

Figure 10: Typical plane wave synthetic seismograms computed for three realizations of 1D stochastic velocity structure. Vertical and radial displacement components are shown. The top traces are for a model containing a layer 30 km thick with an average velocity of 5.5 km/sec and a standard deviation 10% of the average. The center pair of synthetics are for the same crustal model as the top pair but with the addition of a high

velocity (8.0 km sec) halfspace. The arrow points to the Moho Ps conversion on the radial component. The lower pair of synthetics were computed using a layer thickness of 60 km, average velocity of 6 km/sec and velocity standard deviation of 20%. Ps conversions and reverberations start to attain amplitudes seen in the PAS data.

Figure 11: Envelope stack of the three-component data of four earthquakes (see Table 1) recorded at PAS. The envelope is shifted 10 seconds for display purposes. Lines show predicted coda levels for assumption of scattering Q's of 100, 200, 300, and 400 using the wholespace energy flux model (equation 10). Scattering Q at PAS is approximately 200 to 300 but the coda appears to decay slightly faster than predicted by the model.

Figure 12: Coda envelope stacks for the 1D simulation. The "10%" envelope is the stack of 18 vertical and radial synthetic seismograms produced by 9 realizations of the 30 km thick layer model with average velocity of 5.5 km/sec and velocity standard deviation of 10%. The "20%" envelope is the stack of 20 vertical and radial synthetic seismograms produced by 10 realizations of the 60 km thick layer model with average velocity of 6 km/sec and velocity standard deviation of 20%. The straight lines are least-squares fits of the coda. Q_S values are those inferred from the zero lapse time intercept of the linear fits (see text). Note that coda decay in the 1D simulations agree with the assumption that coda energy follows a diffusion law for leaking into the halfspace. Coda decay is controlled entirely by this process in the 1D simulations.

Figure 13: Three component data recorded at SCP (State College, PA) on the DWSSN intermediate-period system (Table 4). Long-period noise seen on some horizontal waveforms (e.g., 08/12/85) was largely removed by the bandpass filter used in this study.

Figure 14: Envelope stacks of the PAS and SCP data showing least-squares fits

of a line through coda with lapse times greater than 10 seconds. Q_S inferred from each lines' zero time intercept is also displayed. Coda excited at PAS attains higher levels and falls off more slowly than coda at SCP.

Figure A1: Amplitude spectra of the nominal Benioff 1-90 response (top) and response differences (lower curves) assuming 30% variation in damping and free periods of the seismometer and galvonometer of the system. Parameters hs, hg, Ts, and Tg are the seismometer damping, galvonometer damping, seismometer period (sec) and galvonometer period, respectively. See text for explanation.

Figure A2: Comparison of Benioff 1-90 three component data from the 02/01/73 event (top) and the 12/28/73 event (bottom). Polarities have been reversed for the vertical (Z) and east-west (E) components of the 12/28/73 event for comparison purposes. The vertical components are simple showing a single impulsive P wave. The arrow shows the location of the major Ps conversion considered in the this study. It occurs primarily on the N component for the 02/01/73 event and on the E component for the 12/28/73 event. Likewise it is not obvious on the other respective horizontal components (right side) showing that both horizontal instruments respond similarly to the same wave propagation effect.

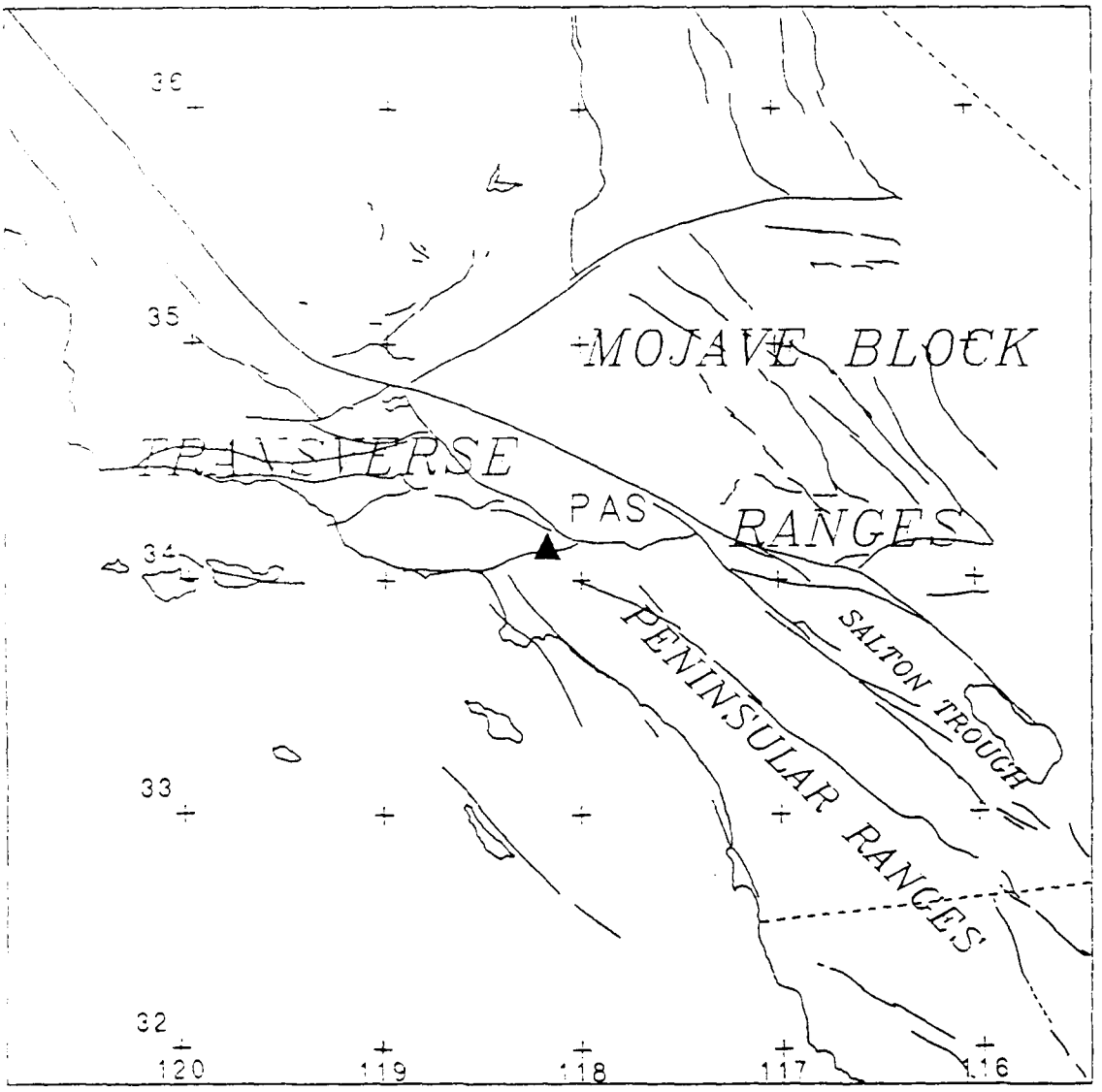
36
35
34
33
32
120
119
118
117
116
MOJAVE BLOCK
TRANSVERSE
RANGES
PAS
SALTON TROUGH
PENINSULAR RANGES

FIG. 1

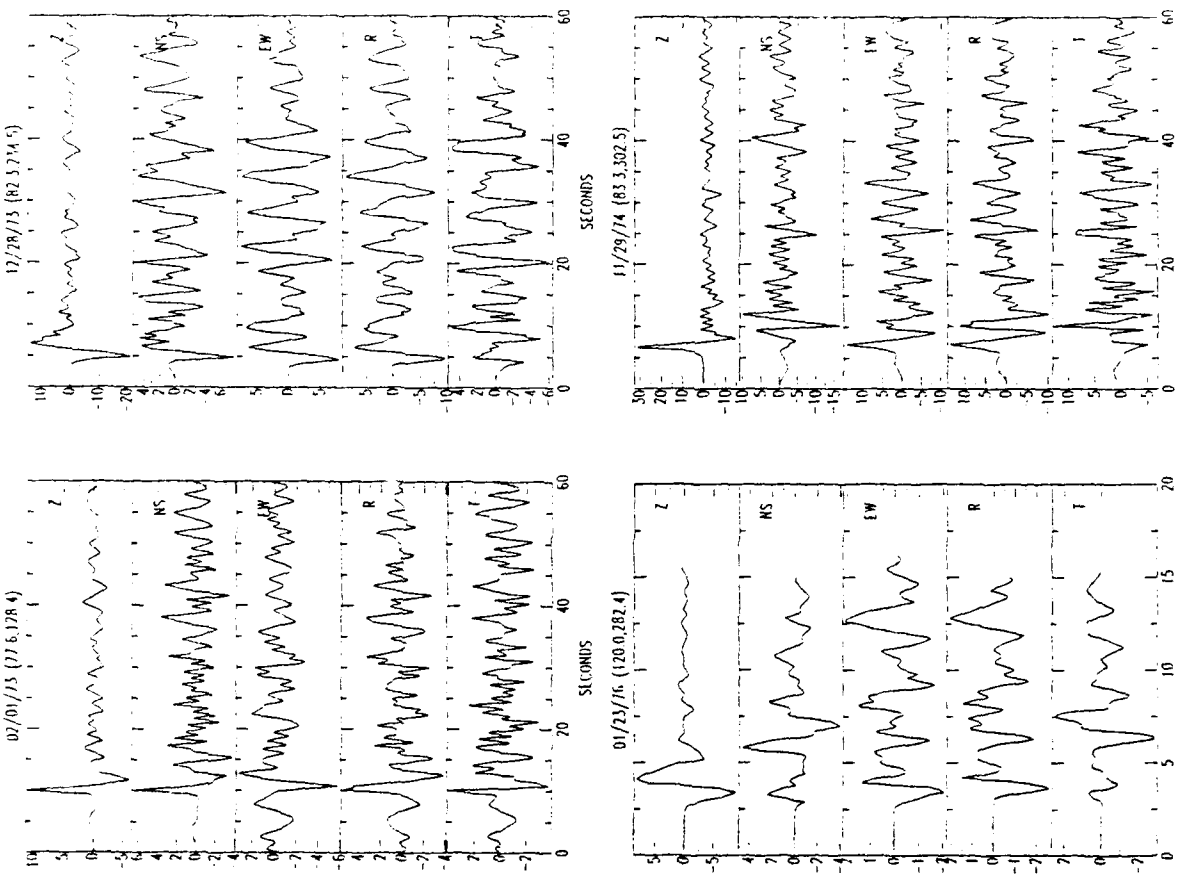
12/28/15 (82 5 214 5)
11/29/14 (83 3, 302 5)
02/01/15 (21 6, 128 4)
01/23/16 (120 0, 282 4)
Z
NS
EW
R
T
SECONDS

FIG. 2

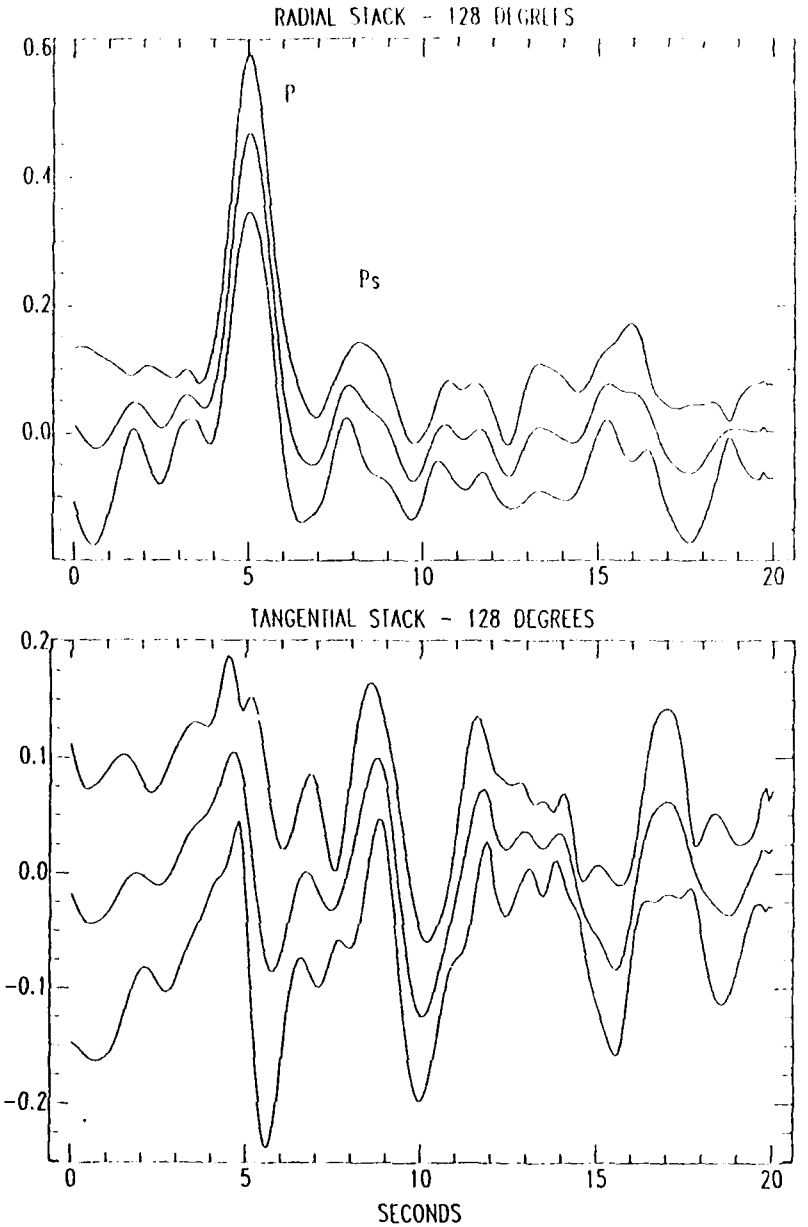
RADIAL STACK - 128 DEGREES
0.6
0.4
0.2
0.0
P
Ps
0
5
10
15
20
TANGENTIAL STACK - 128 DEGREES
0.2
0.1
0.0
-0.1
-0.2
0
5
10
15
20
SECONDS

FIG. 3a

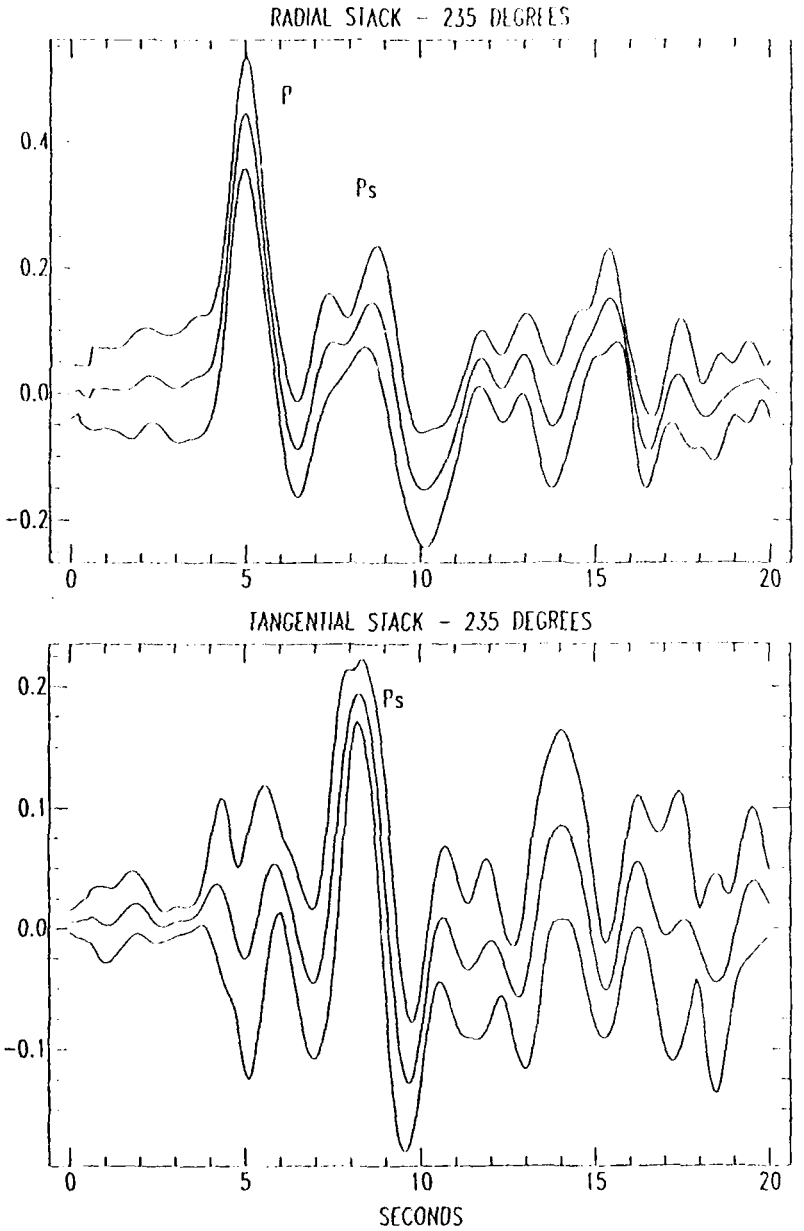
RADIAL STACK - 235 DEGREES
P
Ps
0.4
0.2
0.0
-0.2
0
5
10
15
20
TANGENTIAL STACK - 235 DEGREES
Ps
0.2
0.1
0.0
-0.1
0
5
10
15
20
SECONDS

FIG. 36

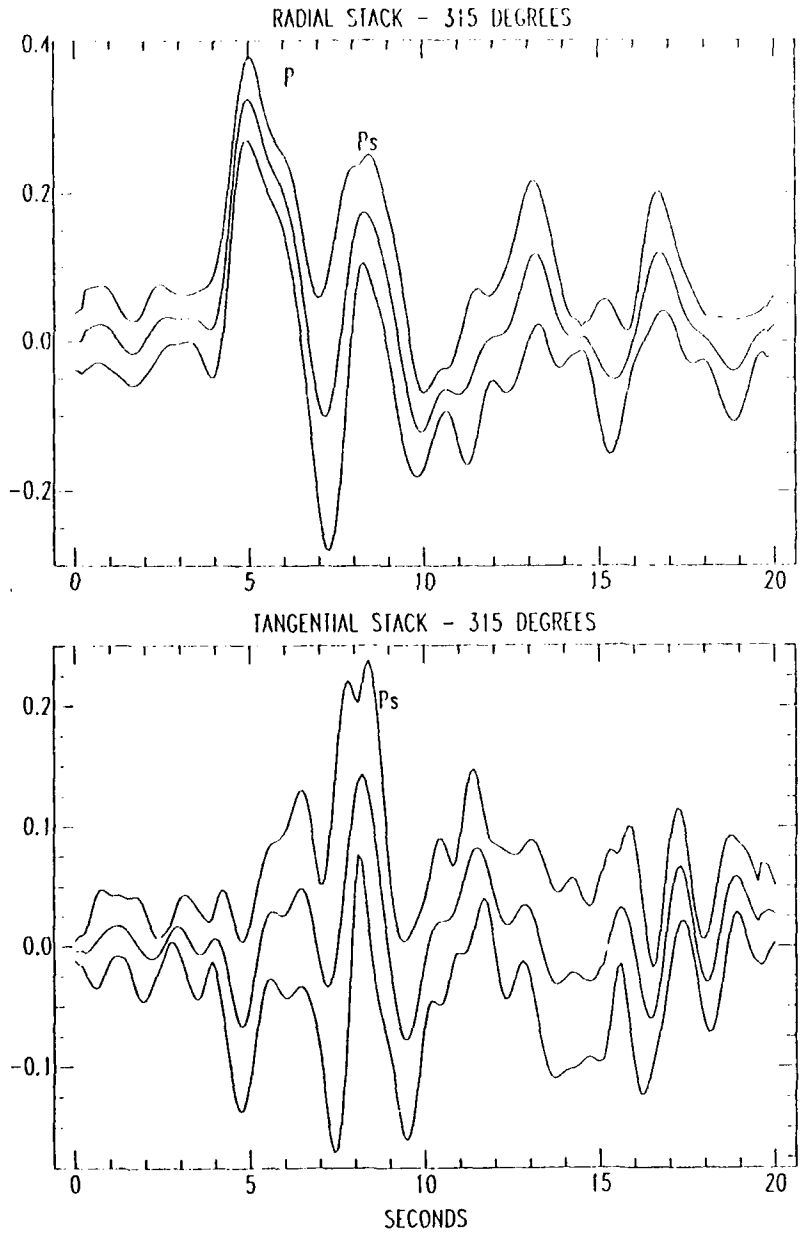
RADIAL STACK - 315 DEGREES
0.4
0.2
0.0
-0.2
P
Ps
0
5
10
15
20
TANGENTIAL STACK - 315 DEGREES
0.2
0.1
0.0
-0.1
Ps
0
5
10
15
20
SECONDS

Fig. 3c

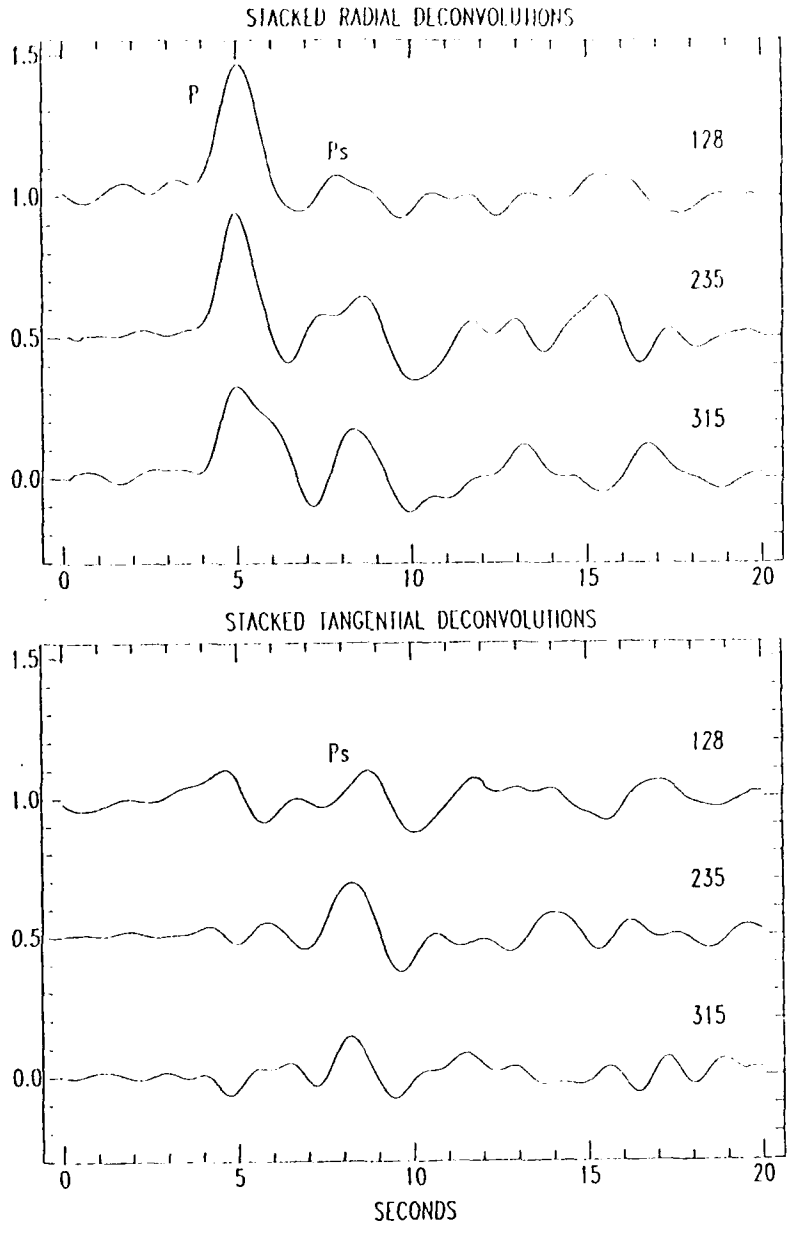
STACKED RADIAL DECONVOLUTIONS
1.5
1.0
0.5
0.0
P
Ps
128
235
315
0
5
10
15
20
STACKED TANGENTIAL DECONVOLUTIONS
1.5
1.0
0.5
0.0
Ps
128
235
315
0
5
10
15
20
SECONDS

FIG. 4

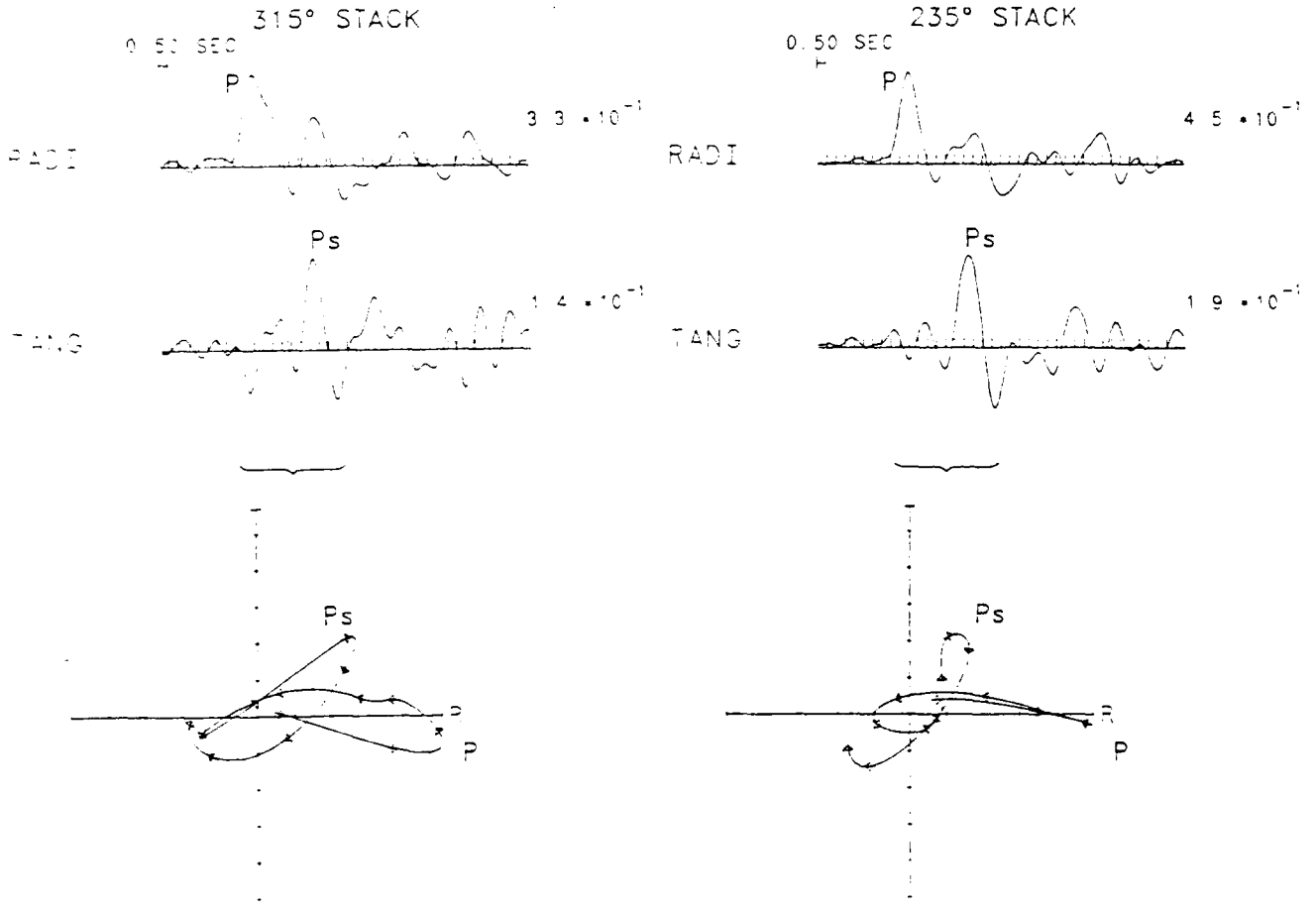
315° STACK
0.50 SEC
P
3.3 • 10⁻¹
RADI
Ps
1.4 • 10⁻¹
TANG
Ps
P
235° STACK
0.50 SEC
P
4.5 • 10⁻¹
RADI
Ps
1.9 • 10⁻¹
TANG
Ps
P

FIG. 5

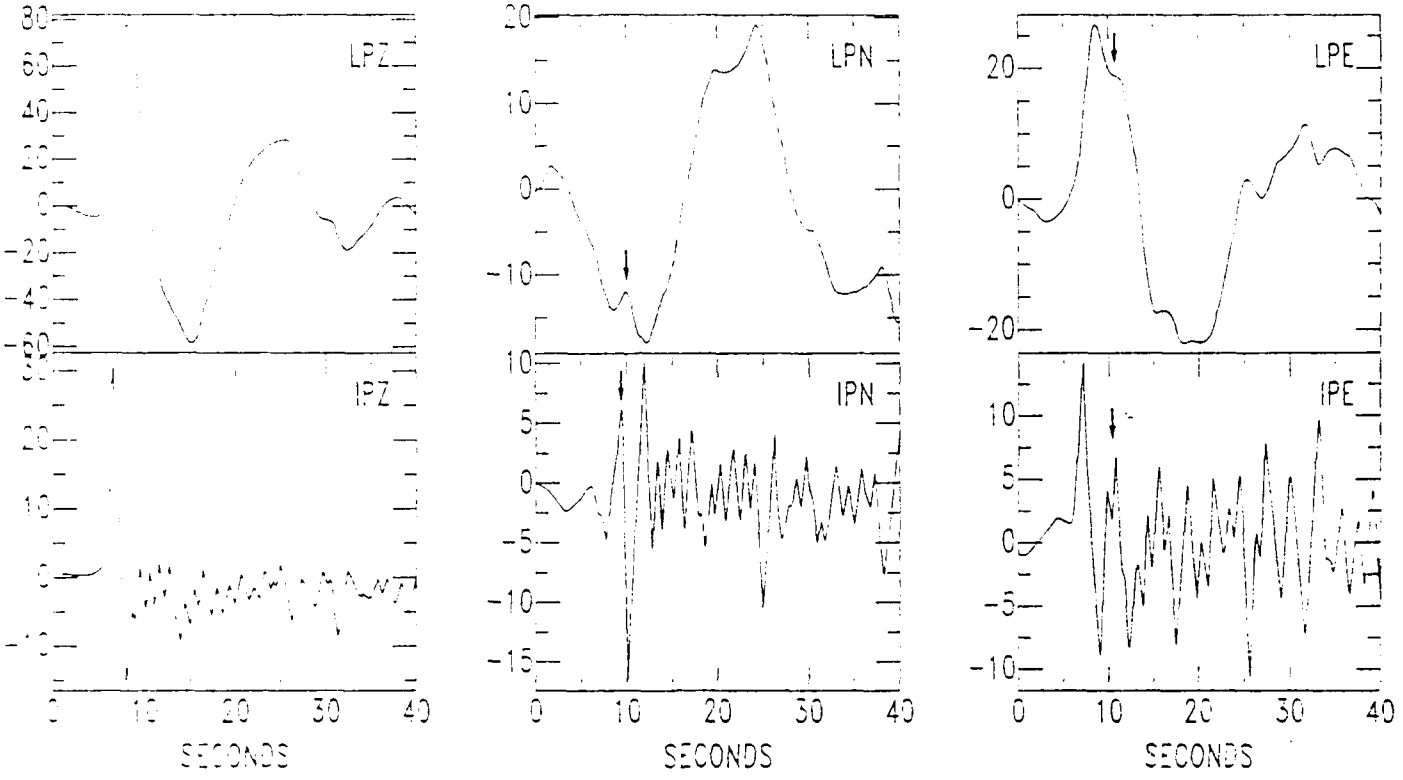

FIG. 6

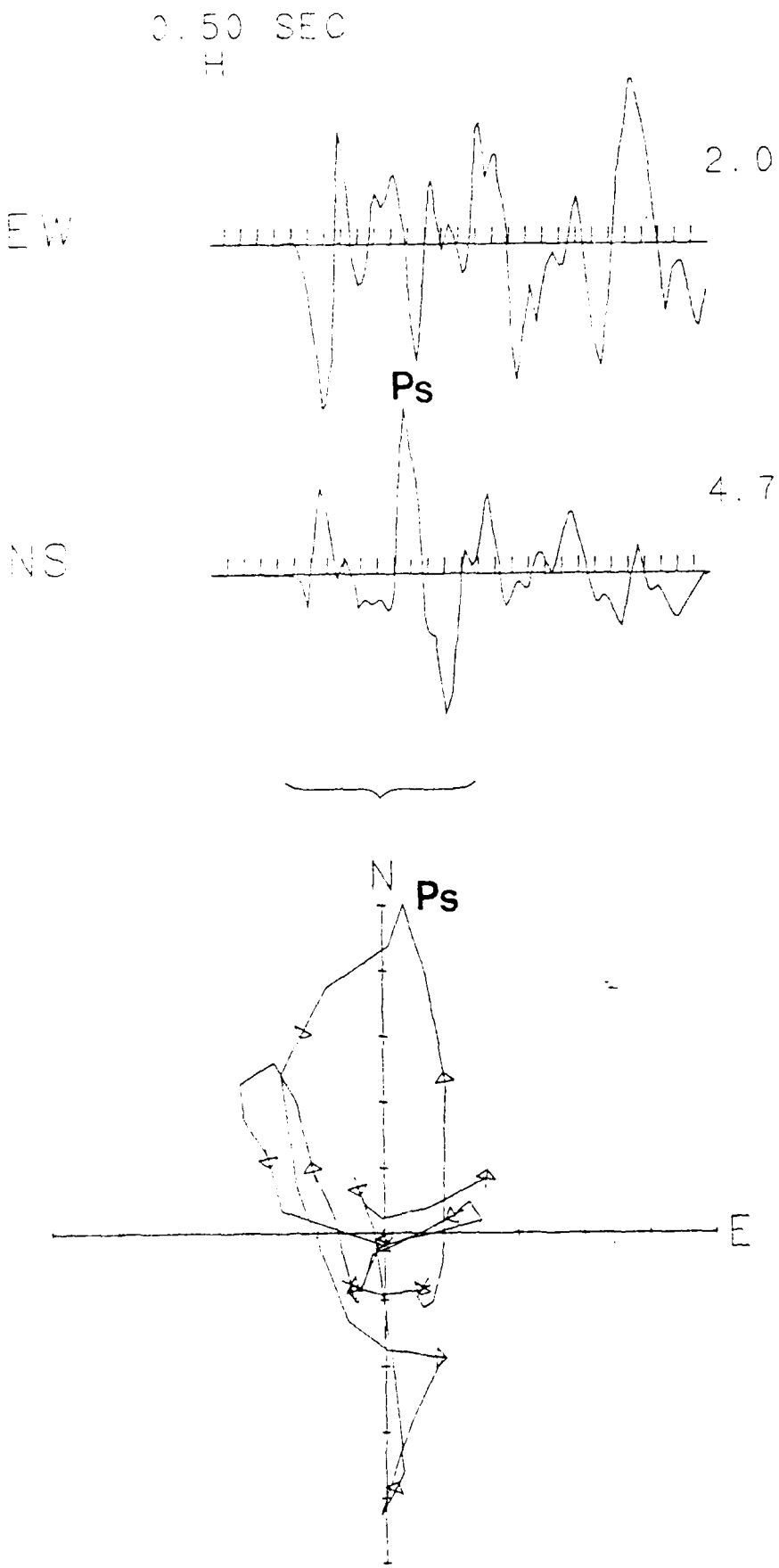

FIG. 7

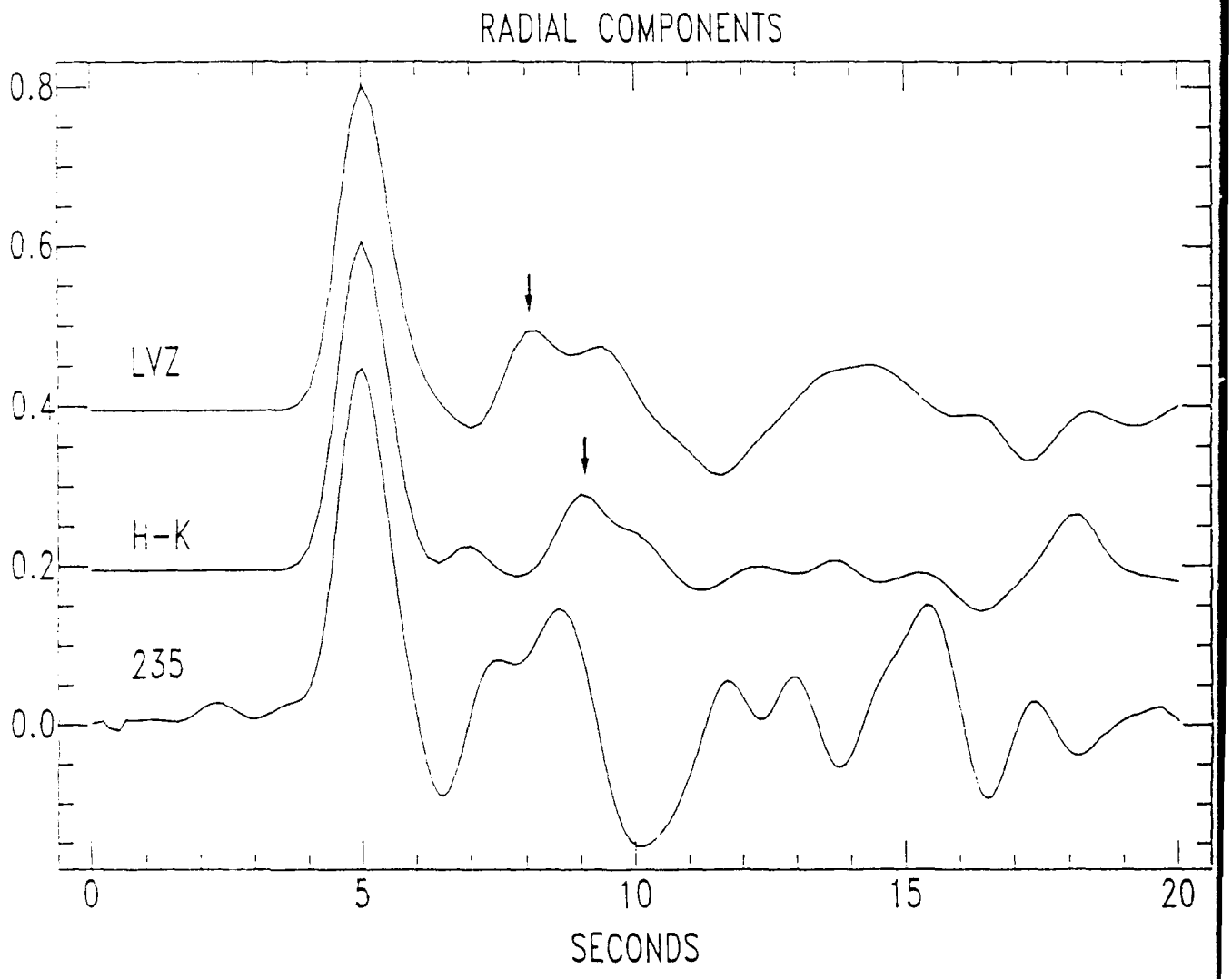

FIG. 8

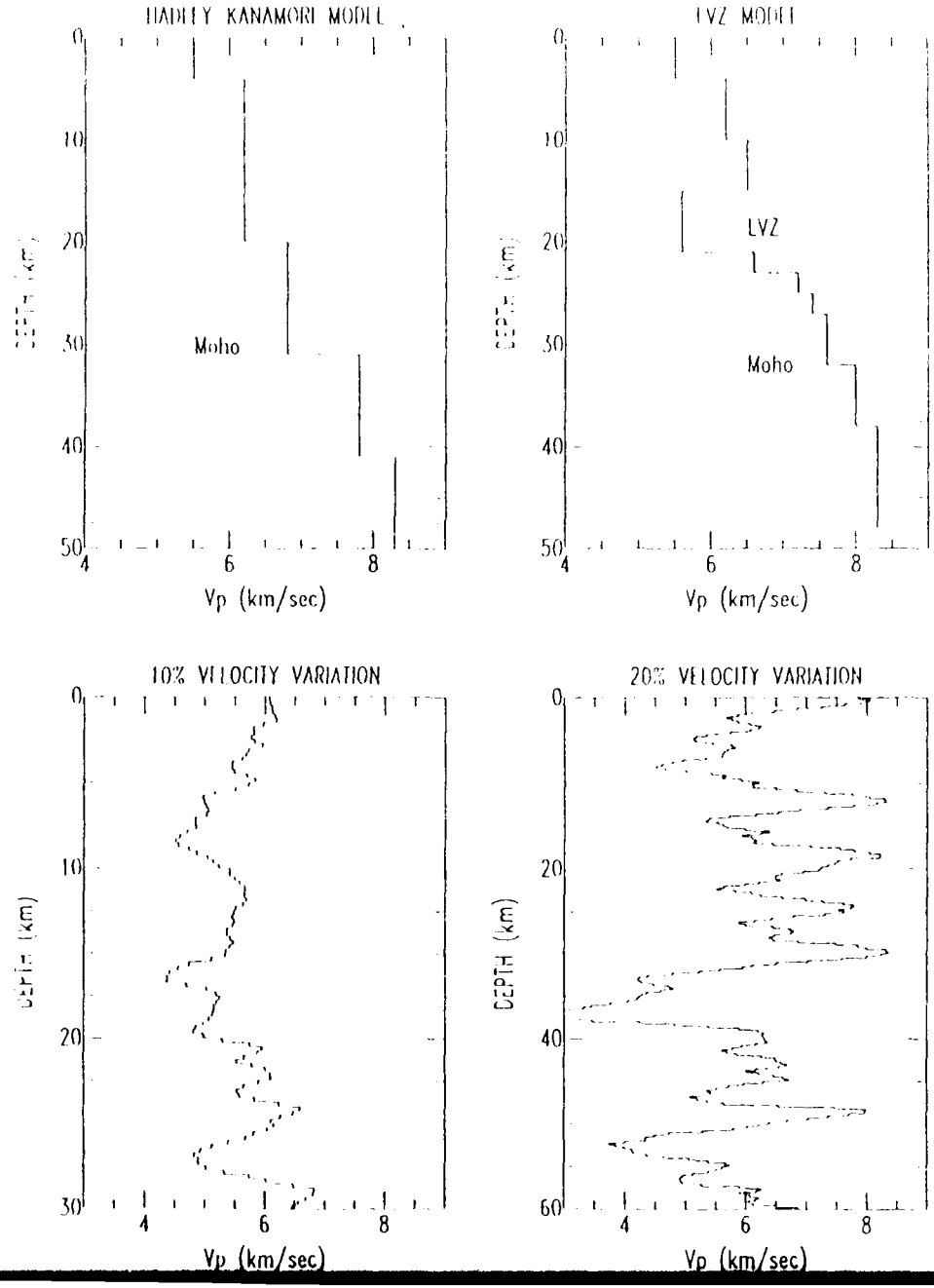
HADLEY KANAMORI MODEL
LVZ MODEL
10% VELOCITY VARIATION
20% VELOCITY VARIATION
Moho
LVZ
Moho
DEPTH (km)
Vp (km/sec)
0
10
20
30
40
50
60
4
6
8

FIG. 9

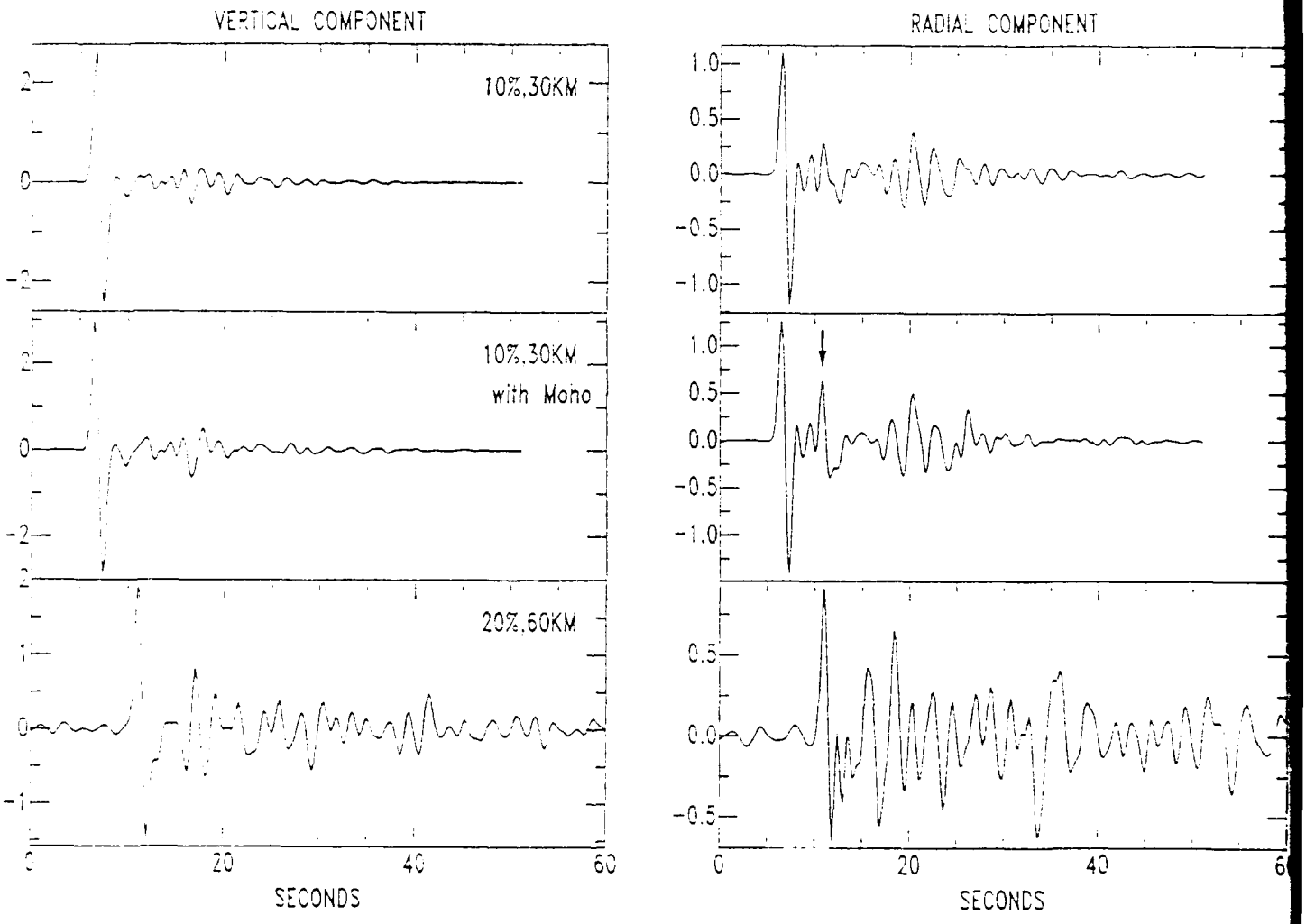
VERTICAL COMPONENT
RADIAL COMPONENT
10%,30KM
10%,30KM
with Moho
20%,60KM
SECONDS
SECONDS

FIG. 10

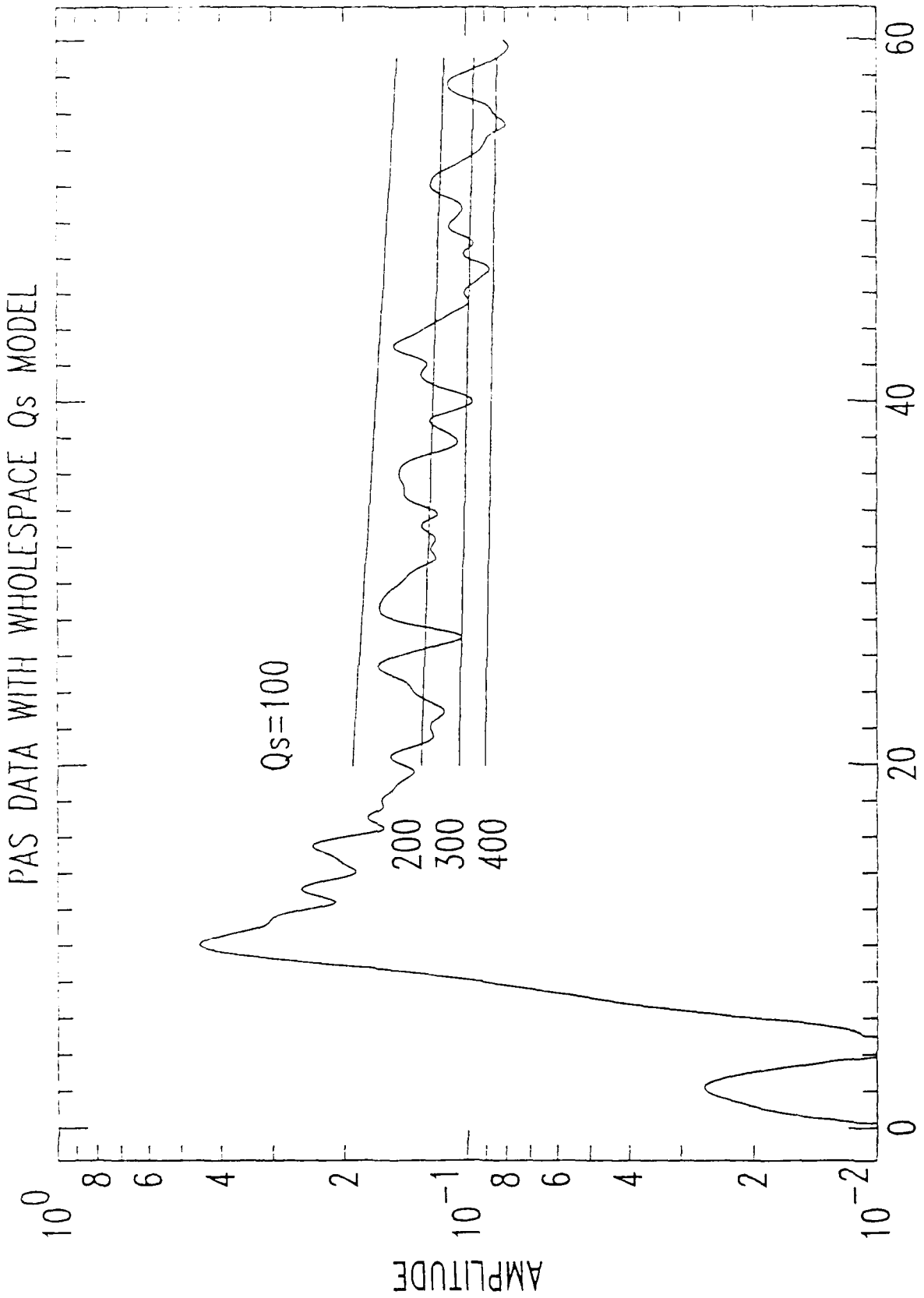
PAS DATA WITH WHOLESPACE Qs MODEL
Qs=100
200
300
400
AMPLITUDE
SECONDS
10^0
8
6
4
2
10^{-1}
8
6
4
2
10^{-2}
0
20
40
60

FIG. 11

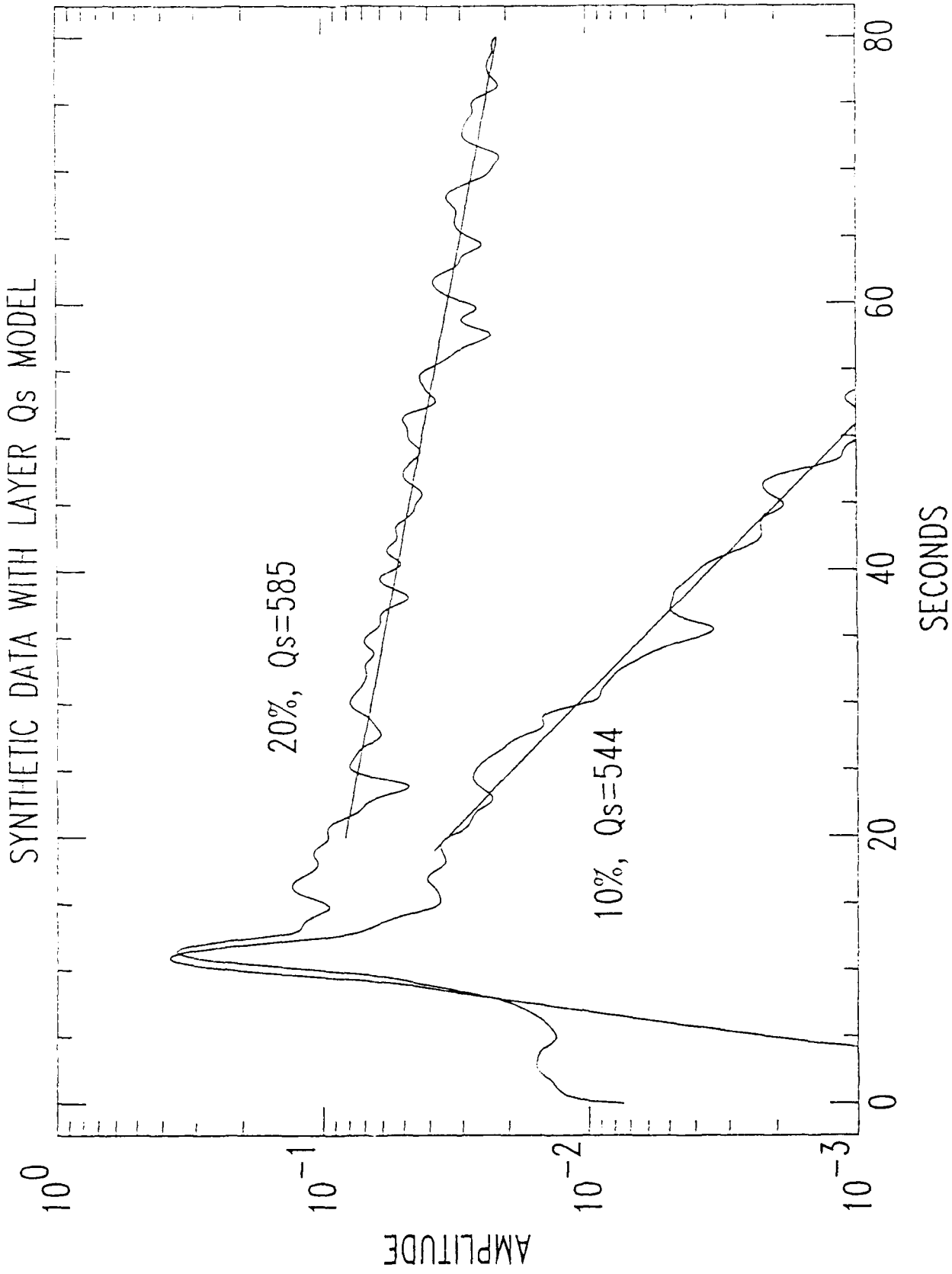
SYNTHETIC DATA WITH LAYER Qs MODEL
20%, Qs=585
10%, Qs=544
AMPLITUDE
SECONDS
10^{0}
10^{-1}
10^{-2}
10^{-3}
0
20
40
60
80

FIG. 12

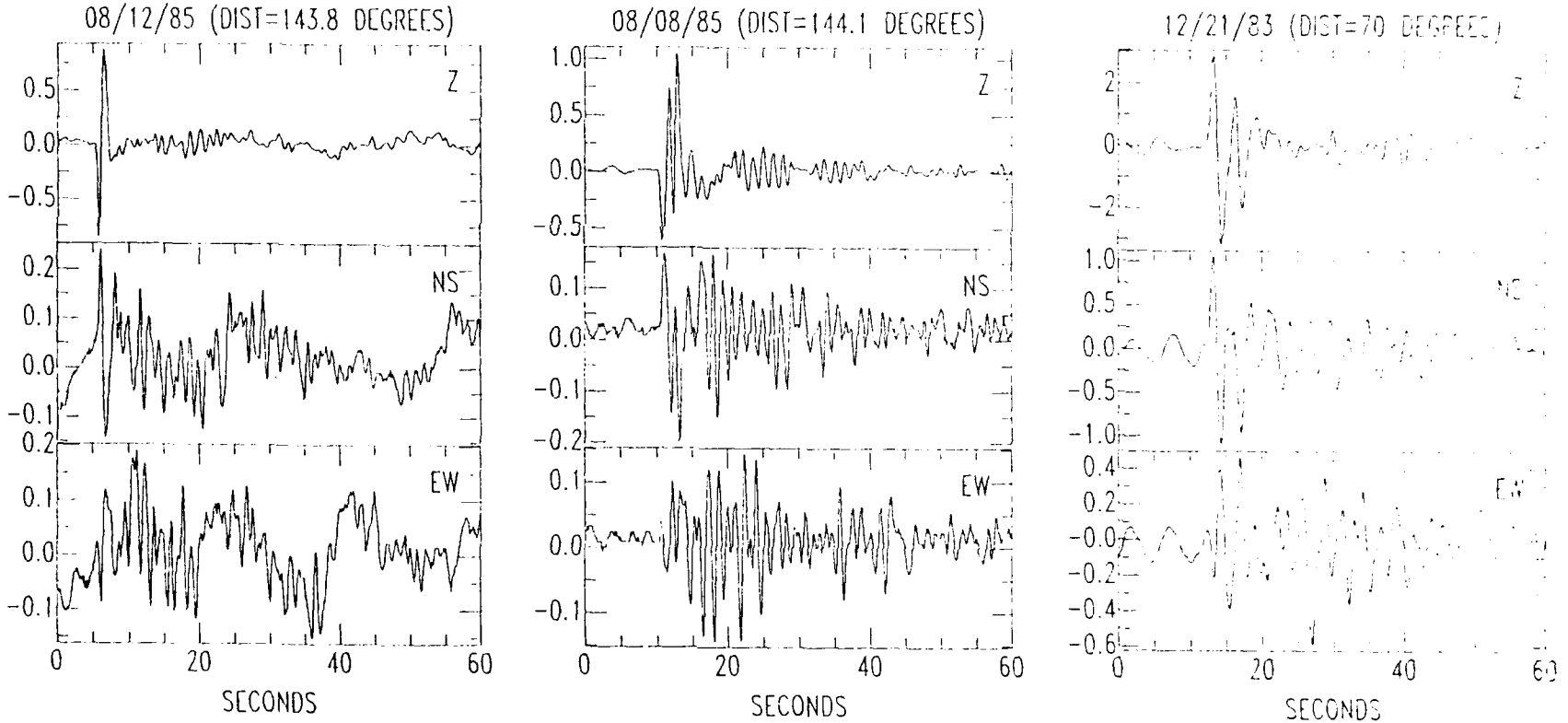
08/12/85 (DIST=143.8 DEGREES)
08/08/85 (DIST=144.1 DEGREES)
12/21/83 (DIST=70 DEGREES)
Z
NS
EW
SECONDS

FIG. 13

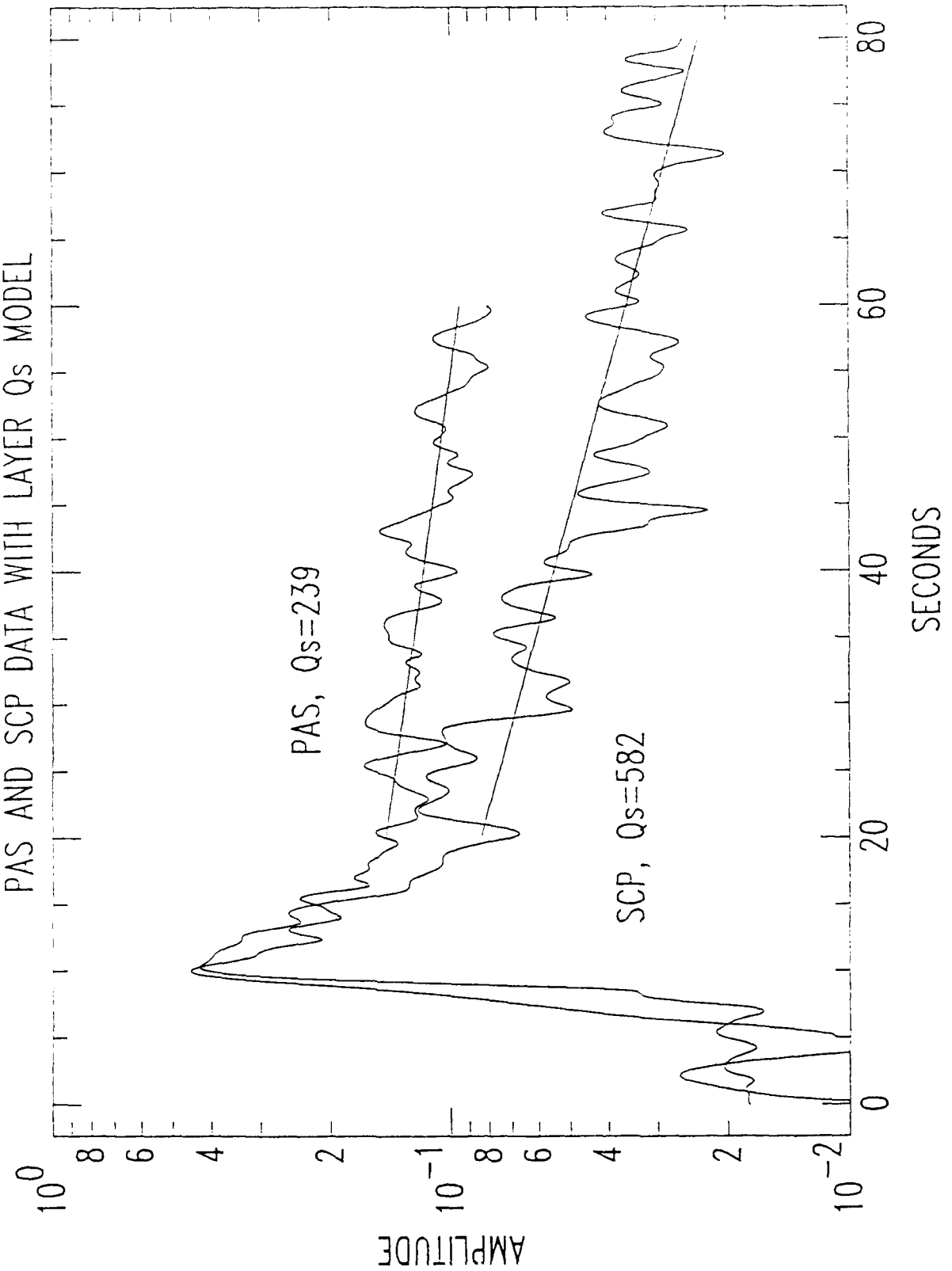
PAS AND SCP DATA WITH LAYER Qs MODEL
PAS, Qs=239
SCP, Qs=582
AMPLITUDE
SECONDS
10^0
8
6
4
2
10^{-1}
8
6
4
2
10^{-2}
0
20
40
60
80

FIG. 14

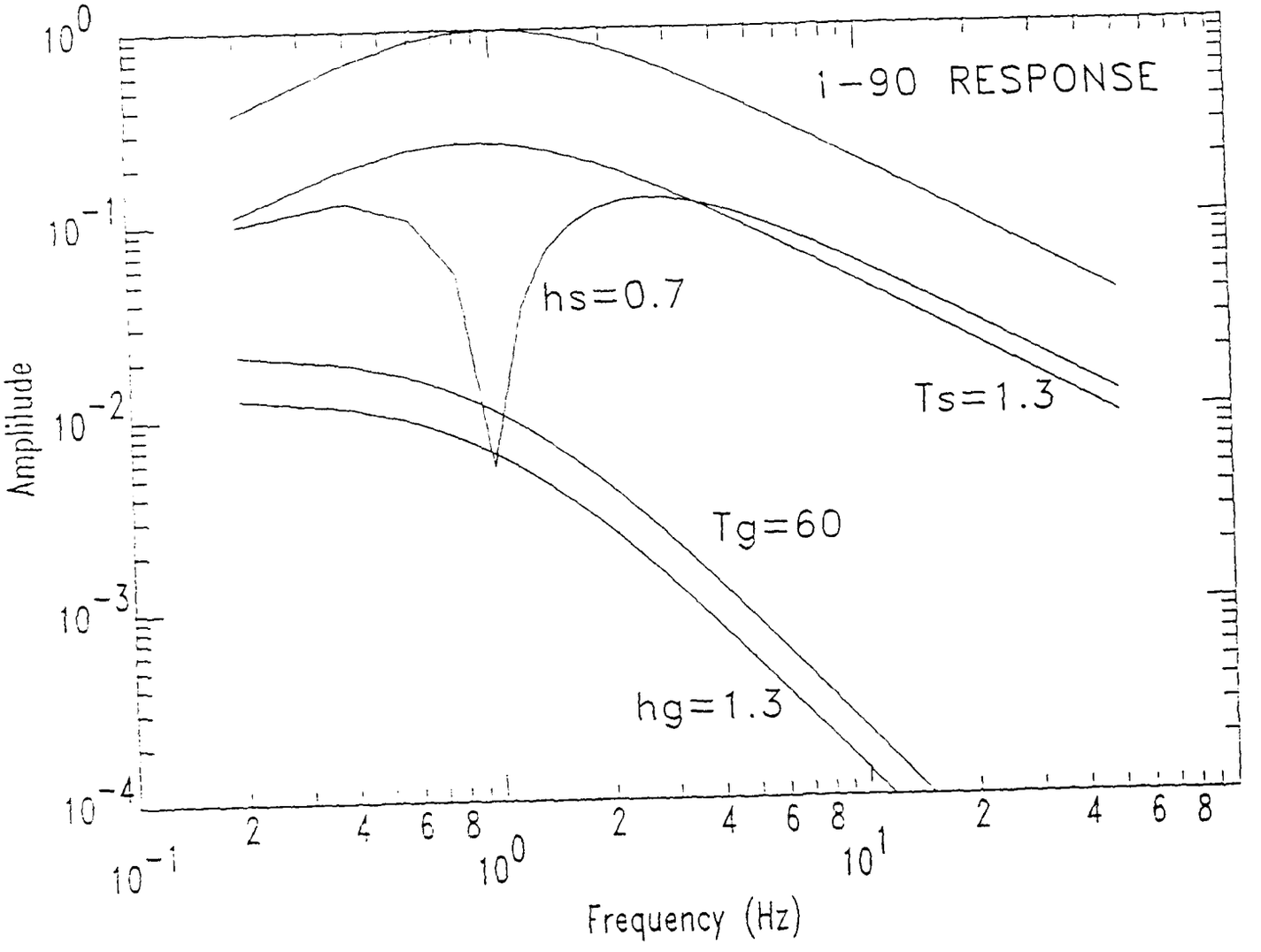
i-90 RESPONSE
hs=0.7
Ts=1.3
Tg=60
hg=1.3
Amplitude
Frequency (Hz)
10^0
10^{-1}
10^{-2}
10^{-3}
10^{-4}
10^{-1}
10^0
10^1
2
4
6
8

FIG. A1

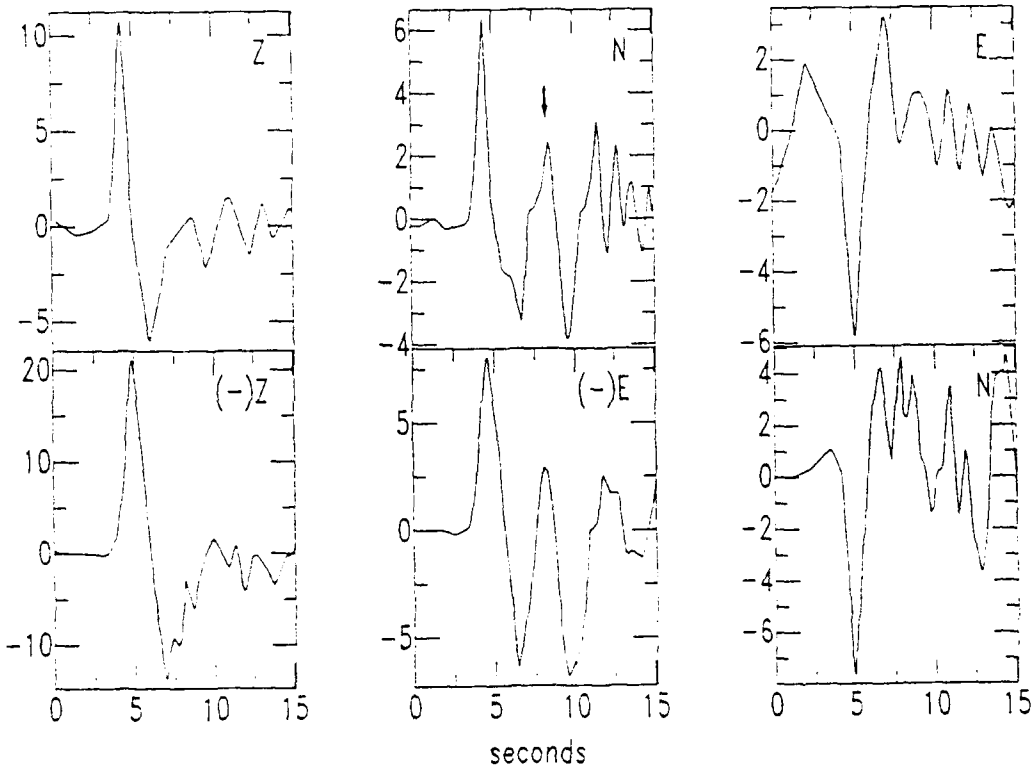

FIG. A2

CONTRACTORS (United States)

Professor Keiiti Aki
Center for Earth Sciences
University of Southern California
University Park
Los Angeles, CA 90089-0741

Professor Charles B. Archambeau
Cooperative Institute for Resch
in Environmental Sciences
University of Colorado
Boulder, CO 80309

Dr. Thomas C. Bache Jr.
Science Applications Int'l Corp.
10210 Campus Point Drive
San Diego, CA 92121 (2 copies)

Dr. Douglas P. Baumgardt
Signal Analysis & Systems Div.
ENSCO, Inc.
5400 Port Royal Road
Springfield, VA 22151-2388

Dr. S. Bratt
Science Applications Int'l Corp.
10210 Campus Point Drive
San Diego, CA 92121

Dr. Lawrence J. Burdick
Woodward-Clyde Consultants
P.O. Box 93245
Pasadena, CA 91109-3245 (2 copies)

Professor Robert W. Clayton
Seismological Laboratory/Div. of
Geological & Planetary Sciences
California Institute of Technology
Pasadena, CA 91125

Dr. Vernon F. Cormier
Department of Geology & Geophysics
U-45, Roon 207
The University of Conneticut
Storrs, Connecticut 06268

Dr. Zoltan A. Der
ENSCO, Inc.
5400 Port Royal Road
Springfield, VA 22151-2388

Professor John Ferguson
Center for Lithospheric Studies
The University of Texas at Dallas
P.O. Box 830688
Richardson, TX 75083-0688

Professor Stanley Flatte'
Applied Sciences Building
University of California, Santa Cruz
Santa Cruz, CA 95064

Professor Steven Grand
Department of Geology
245 Natural History Building
1301 West Green Street
Urbana, IL 61801

Professor Roy Greenfield
Geosciences Department
403 Deike Building
The Pennsylvania State University
University Park, PA 16802

Professor David G. Harkrider
Seismological Laboratory
Div of Geological & Planetary Sciences
California Institute of Technology
Pasadena, CA 91125

Professor Donald V. Helmberger
Seismological Laboratory
Div of Geological & Planetary Sciences
California Institute of Technology
Pasadena, CA 91125

Professor Eugene Herrin
Institute for the Study of Earth
& Man/Geophysical Laboratory
Southern Methodist University
Dallas, TX 75275

Professor Robert B. Herrmann
Department of Earth & Atmospheric
Sciences
Saint Louis University
Saint Louis, MO 63156

Professor Lane R. Johnson
Seismographic Station
University of California
Berkeley, CA 94720

Professor Thomas H. Jordan
Department of Earth, Atmospheric
and Planetary Sciences
Mass Institute of Technology
Cambridge, MA 02139

Dr. Alan Kafka
Department of Geology &
Geophysics
Boston College
Chestnut Hill, MA 02167

Professor Leon Knopoff
University of California
Institute of Geophysics
& Planetary Physics
Los Angeles, CA 90024

Professor Charles A. Langston
Geosciences Department
403 Deike Building
The Pennsylvania State University
University Park, PA 16802

Professor Thorne Lay
Department of Geological Sciences
1006 C.C. Little Building
University of Michigan
Ann Harbor, MI 48109-1063

Dr. Randolph Martin III
New England Research, Inc.
P.O. Box 857
Norwich, VT 05055

Dr. Gary McCartor
Mission Research Corp.
735 State Street
P.O. Drawer 719
Santa Barbara, CA 93102 (2 copies)

Professor Thomas V. McEvilly
Seismographic Station
University of California
Berkeley, CA 94720

Dr. Keith L. McLaughlin
S-CUBED,
A Division of Maxwell Laboratory
P.O. Box 1620
La Jolla, CA 92038-1620

Professor William Menke
Lamont-Doherty Geological Observatory
of Columbia University
Palisades, NY 10964

Professor Brian J. Mitchell
Department of Earth & Atmospheric
Sciences
Saint Louis University
Saint Louis, MO 63156

Mr. Jack Murphy
S-CUBED
A Division of Maxwell Laboratory
11800 Sunrise Valley Drive
Suite 1212
Reston, VA 22091 (2 copies)

Professor J. A. Orcutt
Institute of Geophysics and Planetary
Physics, A-205
Scripps Institute of Oceanography
Univ. of California, San Diego
La Jolla, CA 92093

Professor Keith Priestley
University of Nevada
Mackay School of Mines
Reno, NV 89557

Wilmer Rivers
Teledyne Geotech
314 Montgomery Street
Alexandria, VA 22314

Professor Charles G. Sammis
Center for Earth Sciences
University of Southern California
University Park
Los Angeles, CA 90089-0741

Dr. Jeffrey L. Stevens
S-CUBED,
A Division of Maxwell Laboratory
P.O. Box 1620
La Jolla, CA 92038-1620

Professor Brian Stump
Institute for the Study of Earth & Man
Geophysical Laboratory
Southern Methodist University
Dallas, TX 75275

Professor Ta-liang Teng
Center for Earth Sciences
University of Southern California
University Park
Los Angeles, CA 90089-0741

Professor M. Nafi Toksoz
Earth Resources Lab
Dept of Earth, Atmospheric and
Planetary Sciences
Massachusetts Institute of Technology
42 Carleton Street
Cambridge, MA 02142

Professor Terry C. Wallace
Department of Geosciences
Building #11
University of Arizona
Tucson, AZ 85721

Weidlinger Associates
ATTN: Dr. Gregory Wojcik
620 Hansen Way, Suite 100
Palo Alto, CA 94304

Professor Francis T. Wu
Department of Geological Sciences
State University of new York
At Binghamton
Vestal, NY 13901

OTHERS (United States)

Dr. Monem Abdel-Gawad
Rockwell Internat'l Science Center
1049 Camino Dos Rios
Thousand Oaks, CA 91360

Professor Shelton S. Alexander
Geosciences Department
403 Deike Building
The Pennsylvania State University
University Park, PA 16802

Dr. Ralph Archuleta
Department of Geological
Sciences
Univ. of California at
Santa Barbara
Santa Barbara, CA

Dr. Muawia Barazangi
Geological Sciences
Cornell University
Ithaca, NY 14853

J. Barker
Department of Geological Sciences
State University of New York
at Binghamton
Vestal, NY 13901

Mr. William J. Best
907 Westwood Drive
Vienna, VA 22180

Dr. N. Biswas
Geophysical Institute
University of Alaska
Fairbanks, AK 99701

Dr. G. A. Bollinger
Department of Geological Sciences
Virginia Polytechnical Institute
21044 Derring Hall
Blacksburg, VA 24061

Dr. James Bulau
Rockwell Int'l Science Center
1049 Camino Dos Rios
P.O. Box 1085
Thousand Oaks, CA 91360

Mr. Roy Burger
1221 Serry Rd.
Schenectady, NY 12309

Dr. Robert Burridge
Schlumberger-Doll Resch Ctr.
Old Quarry Road
Ridgefield, CT 06877

Science Horizons, Inc.
ATTN: Dr. Theodore Cherry
710 Encinitas Blvd., Suite 101
Encinitas, CA 92024 (2 copies)

Professor Jon F. Claerbout
Professor Amos Nur
Dept. of Geophysics
Stanford University
Stanford, CA 94305 (2 copies)

Dr. Anton W. Dainty
AFGL/LWH
Hanscom AFB, MA 01731

Professor Adam Dziewonski
Hoffman Laboratory
Harvard University
20 Oxford St.
Cambridge, MA 02138

Professor John Ebel
Dept of Geology & Geophysics
Boston College
Chestnut Hill, MA 02167

Dr. Alexander Florence
SRI International
333 Ravenswood Avenue
Menlo Park, CA 94025-3493

Dr. Donald Forsyth
Dept. of Geological Sciences
Brown University
Providence, RI 02912

Dr. Anthony Gangi
Texas A&M University
Department of Geophysics
College Station, TX 77843

Dr. Freeman Gilbert
Institute of Geophysics &
Planetary Physics
Univ. of California, San Diego
P.O. Box 109
La Jolla, CA 92037

Mr. Edward Giller
Pacific Sierra Research Corp.
1401 Wilson Boulevard
Arlington, VA 22209

Dr. Jeffrey W. Given
Sierra Geophysics
11255 Kirkland Way
Kirkland, WA 98033

Dr. Henry L. Gray
Associate Dean of Dedman College
Department of Statistical Sciences
Southern Methodist University
Dallas, TX 75275

Rong Song Jih
Teledyne Geotech
314 Montgomery Street
Alexandria, Virginia 22314

Professor F.K. Lamb
University of Illinois at
Urbana-Champaign
Department of Physics
1110 West Green Street
Urbana, IL 61801

Dr. Arthur Lerner-Lam
Lamont-Doherty Geological Observatory
of Columbia University
Palisades, NY 10964

Dr. L. Timothy Long
School of Geophysical Sciences
Georgia Institute of Technology
Atlanta, GA 30332

Dr. Peter Malin
University of California at Santa Barbara
Institute for Central Studies
Santa Barbara, CA 93106

Dr. George R. Mellman
Sierra Geophysics
11255 Kirkland Way
Kirkland, WA 98033

Dr. Bernard Minster
Institute of Geophysics and Planetary
Physics, A-205
Scripps Institute of Oceanography
Univ. of California, San Diego
La Jolla, CA 92093

Dr. Geza Nagy
SRI International
333 Ravenswood Avenue
Menlo Park, CA 94025-3493

Dr. Jack Oliver
Department of Geology
Cornell University
Ithaca, NY 14850

Dr. Robert Phinney/Dr. F.A. Dahlen
Dept of Geological
Geophysical Sci. University
Princeton University
Princeton, NJ 08540 (2 copies)

RADIX Systems, Inc.
Attn: Dr. Jay Pulli
2 Taft Court, Suite 203
Rockville, Maryland 20850

Professor Paul G. Richards
Lamont-Doherty Geological
Observatory of Columbia Univ.
Palisades, NY 10964

Dr. Norton Rimer
S-CUBED
A Division of Maxwell Laboratory
P.O. 1620
La Jolla, CA 92038-1620

Professor Larry J. Ruff
Department of Geological Sciences
1006 C.C. Little Building
University of Michigan
Ann Arbor, MI 48109-1063

Dr. Alan S. Ryall, Jr.
Center of Seismic Studies
1300 North 17th Street
Suite 1450
Arlington, VA 22209-2308 (4 copies)

Dr. Richard Sailor
TASC Inc.
55 Walkers Brook Drive
Reading, MA 01867

Dr. David G. Simpson
Lamont-Doherty Geological Observ.
of Columbia University
Palisades, NY 10964

Dr. Bob Smith
Department of Geophysics
University of Utah
1400 East 2nd South
Salt Lake City, UT 84112

Dr. S. W. Smith
Geophysics Program
University of Washington
Seattle, WA 98195

Rondout Associates
ATTN: Dr. George Sutton,
Dr. Jerry Carter, Dr. Paul Pomeroy
P.O. Box 224
Stone Ridge, NY 12484 (4 copies)

Dr. L. Sykes
Lamont Doherty Geological Observ.
Columbia University
Palisades, NY 10964

Dr. Pradeep Talwani
Department of Geological Sciences
University of South Carolina
Columbia, SC 29208

Dr. R. B. Tittmann
Rockwell International Science Center
1049 Camino Dos Rios
P.O. Box 1085
Thousand Oaks, CA 91360

Professor John H. Woodhouse
Hoffman Laboratory
Harvard University
20 Oxford St.
Cambridge, MA 02138

Dr. Gregory B. Young
ENSCO, Inc.
5400 Port Royal Road
Springfield, VA 22151-2388

OTHERS (FOREIGN)

Dr. Peter Basham
Earth Physics Branch
Geological Survey of Canada
1 Observatory Crescent
Ottawa, Ontario
CANADA K1A 0Y3

Dr. Eduard Berg
Institute of Geophysics
University of Hawaii
Honolulu, HI 96822

Dr. Michel Bouchon - Universite
Scientifique et Medicale de Grenob
Lab de Geophysique - Interne et
Tectonophysique - I.R.I.G.M-B.P.
38402 St. Martin D'Heres
Cedex FRANCE

Dr. Hilmar Bungum/NTNF/NORSAR
P.O. Box 51
Norwegian Council of Science,
Industry and Research, NORSAR
N-2007 Kjeller, NORWAY

Dr. Michel Campillo
I.R.I.G.M.-B.P. 68
38402 St. Martin D'Heres
Cedex, FRANCE

Dr. Kin-Yip Chun
Geophysics Division
Physics Department
University of Toronto
Ontario, CANADA M5S 1A7

Dr. Alan Douglas
Ministry of Defense
Blacknest, Brimpton,
Reading RG7-4RS
UNITED KINGDOM

Dr. Manfred Henger
Fed. Inst. For Geosciences & Nat'l Res.
Postfach 510153
D-3000 Hannover 51
FEDERAL REPUBLIC OF GERMANY

Dr. E. Husebye
NTNF/NORSAR
P.O. Box 51
N-2007 Kjeller, NORWAY

Tormod Kvaerna
NTNF/NORSAR
P.O. Box 51
N-2007 Kjeller, NORWAY

Mr. Peter Marshall, Procurement
Executive, Ministry of Defense
Blacknest, Brimpton,
Reading FG7-4RS
UNITED KINGDOM (3 copies)

Dr. Ben Menaheim
Weizman Institute of Science
Rehovot, ISRAEL 951729

Dr. Svein Mykkeltveit
NTNF/NORSAR
P.O. Box 51
N-2007 Kjeller, NORWAY (3 copies)

Dr. Robert North
Geophysics Division
Geological Survey of Canada
1 Observatory crescent
Ottawa, Ontario
CANADA, K1A 0Y3

Dr. Frode Ringdal
NTNF/NORSAR
P.O. Box 51
N-2007 Kjeller, NORWAY

Dr. Jorg Schlittenhardt
Federal Inst. for Geosciences & Nat'l Res.
Postfach 510153
D-3000 Hannover 51
FEDERAL REPUBLIC OF GERMANY

University of Hawaii
Institute of Geophysics
ATTN: Dr. Daniel Walker
Honolulu, HI 96822

FOREIGN CONTRACTORS

Dr. Ramon Cabre, S.J.
c/o Mr. Ralph Buck
Economic Consular
American Embassy
APO Miami, Florida 34032

Professor Peter Harjes
Institute for Geophysik
Rhur University/Bochum
P.O. Box 102148 4630 Bochum 1
FEDERAL REPUBLIC OF GERMANY

Professor Brian L.N. Kennett
Research School of Earth Sciences
Institute of Advanced Studies
G.P.O. Box 4
Canberra 2601
AUSTRALIA

Dr. B. Massinon
Societe Radiomana
27, Rue Claude Bernard
7,005, Paris, FRANCE (2 copies)

Dr. Pierre Mechler
Societe Radiomana
27, Rue Claude Bernard
75005 Paris, FRANCE

GOVERNMENT

Dr. Ralph Alewine III
DARPA/NMRO
1400 Wilson Boulevard
Arlington, VA 22209-2308

Dr. Peter Basham
Geological Survey of Canada
1 Observatory Creseut
Ottowa, Ontario
CANADA K1A 0Y3

Dr. Robert Blandford
DARPA/NMRO
1400 Wilson Boulevard
Arlington, VA 22209-2308

Sandia National Laboratory
ATTN: Dr. H. B. Durham
Albuquerque, NM 87185

Dr. Jack Evernden
USGS-Earthquake Studies
345 Middlefield Road
Menlo Park, CA 94025

U.S. Geological Survey
ATTN: Dr. T. Hanks
Nat'l Earthquake Resch Center
345 Middlefield Road
Menlo Park, CA 94025

Dr. James Hannon
Lawrence Livermore Nat'l Lab.
P.O. Box 808
Livermore, CA 94550

U.S. Arms Control & Disarm. Agency
ATTN: Dick Morrow
Washington, D.C. 20451

Paul Johnson
ESS-4, Mail Stop J979
Los Alamos National Laboratory
Los Alamos, NM 87545

Ms. Ann Kerr
DARPA/NMRO
1400 Wilson Boulevard
Arlington, VA 22209-2308

Dr. Max Koontz
US Dept of Energy/DP 331
Forrestal Building
1000 Independence Ave.
Washington, D.C. 20585

Dr. W. H. K. Lee
USGS
Office of Earthquakes, Volcanoes,
& Engineering
Branch of Seismology
345 Middlefield Rd
Menlo Park, CA 94025

Dr. William Leith
USGS
Mail Stop 928
Reston, VA 22092

Dr. Robert Masse'
Box 25046, Mail Stop 967
Denver Federal Center
Denver, Colorado 80225

R. Morrow
ACDA/VI
Room 5741
320 21st Street N.W
Washington, D.C. 20451

Dr. Keith K. Nakanishi
Lawrence Livermore National Laboratory
P.O. Box 808, L-205
Livermore, CA 94550 (2 copies)

Dr. Carl Newton
Los Alamos National Lab.
P.O. Box 1663
Mail Stop C335, Group E553
Los Alamos, NM 87545

Dr. Kenneth H. Olsen
Los Alamos Scientific Lab.
Post Office Box 1663
Los Alamos, NM 87545

Howard J. Patton
Lawrence Livermore National Laboratory
P.O. Box 808, L-205
Livermore, CA 94550

AFOSR/NP
ATTN: Colonel Jerry J. Perrizo
Bldg 410
Bolling AFB, Wash D.C. 20332-6448

HQ AFTAC/TT
Attn. Dr. Frank F. Pilotte
Patrick AFB, Florida 32925-6001

Mr. Jack Rachlin
USGS - Geology, Rm 3 C136
Mail Stop 928 National Center
Reston, VA 22092

Robert Reinke
AFWL/NTESG
Kirtland AFB, NM 87117-6008

HQ AFTAC/TGR
Attn Dr. George H. Rothe
Patrick AFB, Florida 32925-6001

Donald L. Springer
Lawrence Livermore National Laboratory
P.O. Box 808, L-205
Livermore, CA 94550

Dr. Lawrence Turnbull
OSWR/NED
Central Intelligence Agency
CIA, Room 5G48
Washington, D.C. 20505

Dr. Thomas Weaver
Los Alamos Scientific Laboratory
Los Almos, NM 97544

AFGL/SULL
Research Library
Hanscom AFB, MA 01731-5000 (2 copies)

Secretary of the Air Force (SAFRD)
Washington, DC 20330
Office of the Secretary Defense
DDR & E
Washington, DC 20330

HQ DNA
ATTN: Technical Library
Washington, DC 20305

Director, Technical Information
DARPA
1400 Wilson Blvd.
Arlington, VA 22209

AFGL/XO
Hanscom AFB, MA 01731-5000

AFGL/LW
Hanscom AFB, MA 01731-5000

DARPA/PM
1400 Wilson Boulevard
Arlington, VA 22209

Defense Technical
Information Center
Cameron Station
Alexandria, VA 22314
(12 copies)

Defense Intelligence Agency
Directorate for Scientific &
Technical Intelligence
Washington, D.C. 20301

Defense Nuclear Agency/SPSS
ATTN: Dr. Michael Shore
6801 Telegraph Road
Alexandria, VA 22310

AFTAC/CA (STINFO)
Patrick AFB, FL 32925-6001